Accepted Manuscript

Generation of an *in vitro* 3D PDAC stroma rich spheroid model

Matthew J. Ware, Vazrik Keshishian, Justin J. Law, Jason C. Ho, Carlos A. Favela, Paul Rees, Billie Smith, Sayeeduddin Mohammad, Rosa F. Hwang, Kimal Rajapakshe, Cristian Coarfa, Shixia Huang, Dean P. Edwards, Stuart J. Corr, Biana Godin, PhD, Steven A. Curley

PII: S0142-9612(16)30442-2

DOI: 10.1016/j.biomaterials.2016.08.041

Reference: JBMT 17688

To appear in: *Biomaterials*

Received Date: 19 April 2016

Revised Date: 17 August 2016

Accepted Date: 25 August 2016

Please cite this article as: Ware MJ, Keshishian V, Law JJ, Ho JC, Favela CA, Rees P, Smith B, Mohammad S, Hwang RF, Rajapakshe K, Coarfa C, Huang S, Edwards DP, Corr SJ, Godin B, Curley SA, Generation of an *in vitro* 3D PDAC stroma rich spheroid model, *Biomaterials* (2016), doi: 10.1016/j.biomaterials.2016.08.041.

Generation of an *in vitro* 3D PDAC stroma rich spheroid model

Matthew J. Ware[1], Vazrik Keshishian[1], Justin J. Law[1], Jason C Ho[1], Carlos A Favela[4], Paul Rees[2], Billie Smith[3], Sayeeduddin Mohammad[3], Rosa F. Hwang[7], Kimal Rajapakshe[8], Cristian Coarfa[8], Shixia Huang[8], Dean P. Edwards[8], Stuart J. Corr[1,4,5], Biana Godin#[6] and Steven A. Curley#[1]*

[1]Department of Surgery, Baylor College of Medicine, Houston, Texas, 77030, USA
[2]Department of Engineering, Swansea University, Swansea, United Kingdom
[3]Pathology and Histology Core, Baylor College of Medicine, Houston, Texas, 77030, USA
[4]Department of Systems Medicine and Bio-engineering, Houston Methodist Research Institute, Houston, Texas 77030, USA
[4]Department of Chemistry, Rice University, Houston, TX 77005, USA
[5]Department of Bioengineering, University of Houston, Houston, TX 77204, USA
[6]Department of Nanomedicine, Houston Methodist Research Institute, Houston, Texas 77030, USA
[7]Department of Surgical Oncology, University of Texas MD Anderson Cancer Center, Houston Texas 77030, USA
[8] Department of Molecular and Cell Biology, Baylor College of Medicine, Houston, Texas, 77030, USA.

CORRESPONDING AUTHORS:
Dr. Steven Curley,
Surgery/General Surgery Division
Baylor College of Medicine
One Baylor Plaza,
Houston
Texas, 77030

Dr. Biana Godin
Department of Nanomedicine
Houston Methodist Research Institute
Houston
Texas, 77030
Email: bianagodinv@gmail.com; bgodin@houstonmethodist.org
Phone: 713-4417329

KEYWORDS: *3D tumor microenvironment, Pancreatic Cancer, stroma, human pancreatic stellate cells*

Abstract

Pancreatic ductal adenocarcinoma (PDAC) is characterized by a prominent desmoplastic/stromal reaction, which contributes to the poor clinical outcome of this disease. Therefore, greater understanding of the stroma development and tumor-stroma interactions is highly required. Pancreatic stellate cells (PSC) are myofibroblast-like cells that located in exocrine areas of the pancreas, which as a result of inflammation produced by PDAC migrate and accumulate in the tumor mass, secreting extracellular matrix components and producing the dense PDAC stroma. Currently, only a few orthotopic or ectopic animal tumor models, where PDAC cells are injected into the pancreas or subcutaneous tissue layer, or genetically engineered animals offer tumors that encompass some stromal component. Herein, we report generation of a simple 3D PDAC *in vitro* micro-tumor model without an addition of external extracellular matrix, which encompasses a rich, dense and active stromal compartment. We have achieved this *in vitro* model by incorporating PSCs into 3D PDAC cell culture using a modified hanging drop method. It is now known that PSCs are the principal source of fibrosis in the stroma and interact closely with cancer cells to create a tumor facilitatory environment that stimulates local and distant tumor growth. The 3D micro-stroma models are highly reproducible with excellent uniformity, which can be used for PDAC-stroma interaction analysis and high throughput automated drug-screening assays. Additionally, the increased expression of collagenous regions means that molecular based perfusion and cytostaticity of gemcitabine is decreased in our Pancreatic adenocarcinoma stroma spheroids (PDAC-SS) model when compared to spheroids grown without PSCs. We believe this model will allow an improved knowledge of PDAC biology and has the potential to provide an insight into pathways that may be therapeutically targeted to inhibit PSC activation, thereby inhibiting the development of fibrosis in PDAC and interrupting PSC-PDAC cell interactions so as to inhibit cancer progression.

Pancreatic ductal adenocarcinoma (PDAC) is the fourth leading cause of cancer related death in developed countries[1,2]. Five-year survival is approximately 6% and survival beyond 12 months is unusual. Only 20% of patients are deemed suitable for attempted curative resection. Chemotherapy confers marginal benefit while the benefit of radiotherapy is debated[3]. Despite aggressive research, little improvement in patient survival has occurred in the last decade. In fact, the best chemotherapeutic treatments currently only prolong life by ~6-12 weeks [4]. The poor clinical outcome is attributed, at least in part, to the dense stromal reaction that arises during PDAC development and progression. In support of this notion, it has been shown that sequestration of chemotherapeutic agents such as gemcitabine can occur within the tumor stroma, effectively reducing the amount of the drug that can reach cancer cells [5]

One of the major players in the stromal compartment of PDAC are pancreatic stellate cells (PSCs). Pancreatic stellate cells are resident cells of the pancreas and are predominantly periacinar in location and comprise 4-7% of total pancreatic parenchymal cells. In healthy pancreas, PSCs remain in a quiescent state [6]. PSCs are thought to play a primary role in maintenance of normal pancreatic architecture due to their ability to produce extra-cellular matrix (ECM) proteins as well as the enzymes that regulate ECM protein levels, such as matrix metallo-proteinases (MMPs) and tissue inhibitors of metallo-proteinases (TIMPs). During an acute episode of pancreatic injury, PSCs are activated and express α-smooth muscle *actin* (α-SMA), proliferate, migrate, and secrete excess ECM proteins that lay down a lattice for regenerating epithelial cells. As the injury resolves, activated PSCs are lost through apoptosis[7]. MMPs secreted by the remaining PSCs degrade the excess fibrosis resulting in restitution of normal pancreatic tissue. However, during PDAC, an imbalance between ECM production and degradation results in an extensive and dense desmoplastic/fibrotic stroma produced by activated PSCs in which cancer cells are embedded[8]. Recent studies have alluded to PSCs playing an important role in promoting local growth of PDAC, facilitating regional and distant spread of PDAC cells[9,10], aiding PDAC immune-evasion[11-13], and facilitating a stem cell niche in PDAC, all of which have a major impact on the progression of PDAC and play a role in its high recurrence rate. This has meant that the interactions between PDAC cells and PSCs have become increasingly studied. However, there are currently very limited *in-vitro* options to study these complex

While the importance of these studies is not to be understated, increasing evidence in the literature shows the merits of utilizing 3D *in vitro* models rather than 2D, to replicate more precisely the biophysics of the tumor and surrounding micro-environment [14-16].

Three-dimensional tumor spheroids have been grown by numerous groups which enable more accurate representation of tumor cell behaviors in a more complex 3D setting, which rely on cell-cell interactions, pathogenesis, transport of nutrients and therapeutics, and other important factors. However, current spheroid models do not provide a good model for PDAC, as they have not yet featured the key dense stroma component found in all PDAC tumors *in vivo*. Orthotopic or ectopic animal models, where PSCs and PDAC cells are injected into the pancreas or subcutaneous tissue layer, offer tumors that encompass some stromal component usually lacking PSCs. Genetically engineered animal models, on the other hand, represent more precisely the stroma of PDAC[17]. However, the stroma compartment in these tumors is from an animal origin and these models are resource-intensive and time-consuming to create. Moreover, *in vivo* studies often provide only single end point measurements because visualizing the progress of the tumor and its response to therapies over multiple time points is difficult. These difficulties arise because of the inaccessibility of orthotopic tumors for microscopic methods or the animals needing to be sacrificed for histology analysis. Additionally, significant heterogeneity is seen in stromal reaction development *in vivo* [18]. These reasons lead to difficulty in obtaining mechanistic and time resolved data when studying tumor-stromal reactions in PDAC. It is, therefore, essential that more complex *in-vitro* cellular models that better mimic physiologic conditions within the tumor microenvironment be developed to study PDAC cell-stromal interactions for accurate predictions of drug or radiotherapy efficacy.

The importance of PDAC stroma interactions has been previously realized with the development of models incorporating the co-culture of PDAC and PSCs for a more 'organtypic' approach. For instance the use of 2D monolayer co-cultures [19] and models which incorporate PDAC and PSCs embedded in type I glycosaminoglycan scaffolds and in collagen type I or Matrigel[20] have been developed. We believe that this is specifically the first *in-vitro* model, which uses PSCs co-cultured with PDAC cells whilst employing a simple method to obtain a collagen rich spheroid model without adding any external extracellular matrix components. The PDAC-SS are highly reproducible with excellent uniformity, which

uses a viscosity-inducing agent, methylcellulose for co-culturing both PDAC cell lines[21] and PSCs in various ratios for active stroma production. We believe our PDAC-SS model provides an *in-vitro* model for PDAC stroma rich tumors and will further improve understanding of the interaction of PDAC cells and stromal constituents and the initiation and progression of the stroma commonly found in PDAC.

2.0 Materials and Methods

2. 1. Materials

To prepare media for 3D PDAC-SS formation, cell media specific to the particular cell line (as described below) was supplemented with 20% methylcellulose stock solution. For preparation of methylcellulose stock solution 6 g of autoclaved methylcellulose powder (M0512, Sigma-Aldrich) were dissolved in preheated 250 mL basal medium (60°C) for 20 min. Thereafter, 250 mL of medium (room temperature) containing double the amount of FBS for the particular cell line was added to a final volume of 500 mL and the whole solution was mixed overnight at 4°C. The final stock solution was aliquoted and cleared by centrifugation (5000 rpm for 2h at room temperature). Only the clear, highly viscous supernatant was used for the spheroid formation, which was approximately 90-95% of the stock solution.

2.2. Cell lines

Five human PDAC lines, PANC-1, AsPc-1, BxPC-3, Capan-1 and MIA PaCa-2 cells were obtained from American Type Culture Collection (ATCC, USA). PANC-1 and AsPc-1 cells were maintained in DMEM (Thermo Fischer Scientific, USA) with 10% fetal bovine serum (FBS, Sigma, USA). BxPC-3 was maintained in RPMI-1640 (Thermo Fischer Scientific, USA) medium with 10% FBS, Capan-1 in IMDM medium (Thermo Fischer Scientific, USA) with L-4 mM glutamine and 20% FBS. MIA PaCa-2 was maintained in DMEM (Thermo Fischer Scientific, USA) with 10% FBS and 2.5% horse serum (Thermo Fischer Scientific, USA). 2% penicillin-streptomycin solution (Sigma, USA) was added to the media of all PDAC lines. Derivation of all PDAC cell lines are given by Table 1.

Human pancreatic stellate cells (PSCs) were isolated and prepared as previously described[13]

from residual pancreatic adenocarcinoma specimens from patients undergoing primary surgical resection at The University of Texas M. D. Anderson Cancer Center. All human samples were obtained in accordance with the policies and practices of the Institutional Review Board of The University of Texas M. D. Anderson Cancer Center. Tumor samples were minced and seeded in six-well plates containing 15% FCS/DMEM, l-glutamine (2 mmol/L), penicillin/streptomycin, and amphotericin. Five days later, cells were able to grow out from the tissue clumps. When PSCs grew to confluence, cells were trypsinized and passaged 1:3. Cell purity was determined by immunohistochemistry for alpha-SMA, vimentin, and desmin, as well as morphology (spindle-shaped cells with cytoplasmic extensions) and positive staining with Oil Red O (lipid inclusions were visualized). Further, PSC derived from the pancreatic tumor of a patient who had received no prior therapy before surgery were immortalized using lentiviral vector with human telomerase (hTERT) or SV40 large T antigen (TAg) through plasmids containing TAg (pHIV7-CNPO-TAg) and hTERT (pHIV7-CNPO-hTERT) as previously described in details.[23] PSCs carrying the hTERT or SV40-T were selected in 1 to 3 mg/mL G418 for 3 weeks (Invitrogen). Cells were maintained in DMEM with 10% FBS at 37°C in a humidified atmosphere of 5% CO_2.

Table 1: Donor patient information and cell line characteristics

Cell line	Source	Derivation	Metastasis	Proliferation	Differentiation	Ref.
PANC-1	56 y.o, female	Primary tumor	Yes	52h	Poor	[24]
AsPc-1	62 y.o, female	Ascites	Yes	38-40h	Poor	[25]
MIA PaCa-2	65 y.o, female	Primary tumor	Not described	40h	Poor	[26]
Capan-1	40 y.o, male	Liver metastasis	Yes	Not described	Well	[27]
BxPc-3	61 y.o, male	Primary tumor	No	48-60h	Moderate to poor	[28]

2.3. A modified and improved hanging drop method for 3D PDAC-SS formation

Spheroids were created using a novel approach that we have previously described[21]. Briefly, the approach combined two traditionally used techniques: the hanging-drop

0.24% methylcellulose. 20 μL drops of the 0.24% methylcellulose-culture medium solution containing 20,000 cells were pipetted onto the lid of 100 mm dishes and were inverted over dishes containing 10mL phosphate buffer solution. Cells were counted using the Countess Automated Cell Counter according to the manufacturer's recommendations (Invitrogen, USA). A ratio of 1:2 (PSCs : PDAC cells) were gently mixed using pipette action for PDAC-SS. Hanging drop cultures were incubated under standard culture conditions (5% CO_2, at 37°C) for 7 days, which allowed for adequate sedimentation time. The resultant cell aggregates were harvested by pipetting 10 mL of DMEM plus 10% FBS gently onto the lid where the hanging drop spheroids lay, which caused them to become suspended in the media. Each spheroid was gently caught by a sterile spatula and transferred to a well in a 12 well plate for treatment or imaging.

2.4 Generation of orthotopic PDAC tumors in mice

Animal studies were performed in accordance with the guidelines of the Animal Welfare Act and the Guide for the Care and Use of Laboratory Animals based on approved protocols by Baylor College of Medicine Institutional Animal Care and Use Committee (IACUC). Orthotopic pancreatic tumors were grown in 6-7 week old athymic nude (FOXn1 nu) female mice (Harlan Sprague Dawley, USA). Under sterile conditions an incision of ~2 cm was made in the left flank to expose the pancreas. PANC-1 or Capan-1 cells (1 x 10^6 in 40 μL of PBS) were injected into the pancreas. The abdominal wound was closed in two layers. Tumors were allowed to grow for 5 weeks before tumors were excised. The tumor size was measured (average size of tumor was 4 x 4 x 3mm) before fixing in 4% formaldehyde for histology preparation.

2.5. Immunohistochemical evaluation

PDAC-SS were fixed in formalin, embedded in histogel™ (Thermo Scientific Richard-Allan Scientific, USA), processed in paraffin blocks and sectioned using standard techniques. PDAC-SS slides were stained with H&E, Ki67 (proliferation, mouse anti human Ki67, Bio-Rad, USA), Picro Sirius (collagen, Picrosirius red, AbCam, USA), Hypoxia-inducible factor 1-alpha (HIF-1-α, hypoxia, AbCam, USA), and Cleaved PARP (anti-cleaved parp AB, Abcam, USA, apoptosis). Histology slides were imaged using Nikon Eclipse

expression of various histology stains.

Quantities of immature and mature collagen in PDAC-SS were quantified using Picro Sirius stain. Picro Sirius stained histology slides were imaged using a Nikon Eclipse TE2000-U microscope fitted with a CoolSNAP HQ^2 color camera (Photometrics™). A MATLAB program was created to calculate the percentage area fraction of picro sirius negative and picro sirius positive regions (See Supplementary Data 1). A threshold was applied to the color image to identify the 'red' pixels segmented based on its RGB profile. This generated a binary image where white pixels represent the red or collagenous areas within the frame. The number of white pixels was divided by the total number of pixels in the image to give the percentage of collagenous pixels within the area. This was repeated for 10 PDAC-SS per group and for 20 frames of Capan-1 and PANC-1 tumors taken from 3 separate mice. The 20 frames were imaged from random areas of each tumor. Regions of both sparse and dense collagen were considered in all groups.

2.6. Scanning electron microscopy (SEM)

PDAC-SS were fixed by washing thrice with 0.1M sodium cacodylate buffer (CDB, Sigma, USA*)* followed by incubation in 2.5% glutaraldehyde (Sigma, USA) for 25 min at room temperature. Spheroids were washed thrice again in 0.1M CDB and subjected to an increasing concentration of ethanol (Thermo Fischer, USA) wash series for dehydration. The spheroids were then incubated in 1:1 t-butanol (Thermo Fischer, USA): ethanol mixture for 5 min and mounted on carbon tape upon an SEM stub. Immediately before imaging the samples were sputter coated with 50% platinum 50% palladium at a thickness of 5±0.2nm to ensure good electrical conductivity.

2.7. Light microscopy

Brightfield imaging for analysis of size distribution and shape of the micro-stroma and was captured at the desired time points using an Nikon Eclipse TE2000-U microscope fitted with a Nikon digital sight DS-Fi1 video camera.

Reverse phase protein array (RPPA) assays were performed as described previously [29,30] with minor modifications. Protein lysates were prepared from the cell culture samples with Tissue Protein Extraction Reagent (TPER; Pierce) supplemented with 450 mM NaCl and a cocktail of protease and phosphatase inhibitors (Roche Life Science). Protein lysates at 0.5 mg/ml of total protein were denatured in SDS sample buffer (Life Technologies) containing 2.5% 2-mercaptoethanol at 100 °C for 8 min. Protein lysates were arrayed onto nitrocellulose-coated slides (Grace Bio-labs, Bend, OR, USA) using an Aushon 2470 Arrayer (Aushon BioSystems, Billerica, MA, USA) with an array format of 960 (experimental and controls) lysates per slide with each sample spotted as technical triplicates (2,880 spots per slide). Slides were blocked for 1 h with I-Block reagent (Applied Biosystems) followed by a 15 min incubation with Re-Blot reagent (Dako) and were loaded on an automated slide stainer Autolink 48 (Dako, Carpinteria, CA, USA) for incubation with primary antibodies. . Antibody binding was detected by fluorescence with a Vectastain-ABC Streptavidin–Biotin Complex (Vector, PK-6100) followed by incubation with the TSA-plus Biotin Amp Reagent diluted at 1:250 (Perkin Elmer, NEL749B001KT) and a 1:50 dilution of LI-COR IRDye 680 Streptavidin (Odyssey) as the detection probe. The total protein content of each spotted lysate was assessed by fluorescent staining with Sypro Ruby Protein Blot Stain for selected subsets of slides (Molecular Probes). Fluorescent-labelled slides were scanned on a GenePix AL4200 scanner, and the images were analyzed with GenePix Pro 7.0 (Molecular Devices). For normalization, raw image intensity of each spot was subtracted from that of negative controls and then divided by total protein values. Tumors with different genetic backgrounds were analyzed separately. Of the 212 validated antibodies included in the RPPA, 143 antibodies detect total protein and 69 detect specific phosphorylated states known to be markers of protein activation. . The validated antibodies represent proteins in various signaling pathways and cell functional groups including growth factor receptors, cell cycle, cell proliferation, apoptosis, EMT, stem cells, DNA damage, cell stress, autophagy, cytokines, protein translation and gene transcriptional activators and repressors. For a complete list of validated antibodies see https://www.bcm.edu/centers/cancer-center/research/shared-resources/antibody-based-proteomics. Significantly differentiated antibodies between experimental groups were determined using a cutoff of $P < 0.05$ (by two-sided Student's t-tests) and FC (fold change) >1.25 (or < 1/1.25). Enriched pathways

2.9 Perfusion and drug efficacy analysis

For perfusion analysis, spheroids were exposed to 0.1μM FITC and fluorescence was tracked over time using a Nikon Eclipse TE2000-U microscope (Photometrics™).For drug efficacy analysis, spheroids were exposed to 100uM of gemcitabine for 24h, then fixed with 4% PFA for 1h. Spheroids were then stained with Ki67 and ClPARP for histological analysis.

Liquid Chromatography Mass spectroscopy- Mass Spectroscopy (LC-MS/MS) was performed to quantify the relative gemcitabine content with spheroids with and without PSCs. One hundred spheroids were harvested from the hanging drop and incubated with 1000μM of gemcitabine for 3h. They were then washed three times with PBS and spun down to form a pellet. To the cell pellets, 500 μL of 4:1 (Methanol :water) with Internal Standard was added. The samples were then probe sonicated for 30 sec. Then the samples were centrifuged for 30 min at 15,000 rpm at 4C. After centrifugation the supernatant was transferred into a new tube and were dried in Speed Vac for 1 hour. The samples were suspended in 200 μl of 50:50(methanol: water). The injection volume for LC-MS is 5 μl.

LC-MS/MS method was developed for Gemcitabine using Agilent 6490 QQQ equipped with an Agilent jet stream source coupled to an Agilent 1290 Infinity UHPLC system. LC conditions: Waters Acquity UPLC BEH C18 column, 1.7 uM (2.1* 100 mm) (Waters, Milford, MA) was used for the analysis. The mobile phase consisted of A: Water with methanol (80:20) with 10 mM ammonium acetate buffer; B: Acetonitrile with water (90:10) with 10 mM ammonium acetate buffer. The injection volume was 5 microL and flow rate was 0.2 mL/min. Gradient used: % B was increased from 5 (initial conditions) to 98% B in 12 min, kept constant at 98% B for 1 min (up to 13 min), returned to initial conditions (5% B) from 13 to 13.1 minutes and kept constant up to 15 minutes for column equilibration to the starting conditions.

The specific MRM transitions used for Gemcitabine compound and the optimized compound dependent MRM parameters, such as, collision energy, and dwell time. The nitrogen drying gas was set with flow rate of 14 l/min at temperature 200 °C. The pressure of the nitrogen nebulizing gas was set at 40 psi. The sheath gas temperature was 300 °C and

pressure RF was set as 100 Volt.

Data acquisition and analysis: A Mass Hunter workstation (version B.06.01) was used for data acquisition. Mass Hunter Qualitative analysis (version B.06.01) and Quantitative analysis (version B.06.01) were used for data processing. The most abundant MRM transitions were selected for each analyte for relative-quantitation.

The relative gemcitabine content was normalized to the total surface area available for drug-spheroid surface contact, as the spheroids with PSCs tend to have a smaller diameter when compared to spheroids without PSCs.

Structural integrity of PANC-1 spheroids with and without PSCs was quantified using ImageJ analysis software 1.49U (National Institute of Health, USA). Histology images were transformed into binary format before measuring circularity and solidity of their structures. These parameters would give a quantitative measure of the spheroids structural integrity before and after gemcitabine exposure.

Circularity is defined as:

$$4\pi \frac{area\ of\ spheroid}{perimeter\ of\ spheroid^2} \quad (1)$$

A value of 1.0 indicates a perfect circle. As the value approaches 0.0, it indicates an increasingly elongated polygon.

Solidity is defined as:

$$\frac{Area\ of\ spheroid}{convex\ area} \quad (2)$$

Ki67 expression before and after 24h of gemcitabine exposure was quantified from histological color images captured using a Nikon Eclipse TE2000-U microscope fitted with a CoolSNAP HQ^2 color camera (Photometrics™). ImageJ software (National Institute of Health, USA) was used to perform an intensity per unit area measure to quantify the amount of Ki67 present within the spheroids, since Ki67 positive nuclei stain dark brown and negative remain light blue.

3.0 Results

We first cultured PDAC cells and PSCs in 2D monolayer. The base media for PANC-1 and PSCs is DMEM plus 10 and 15% FBS, respectively. However the base media for Capan-1 differs from PSCs (IMDM plus 20% FBS). By co-culturing PDAC and PSCs (2:1 ratio) cell lines in DMEM plus 15% FBS we established that both cell lines can be co-cultured with good viability in the same media. A 2:1 ratio of PDAC to PSCs was chosen after investigation of the effectiveness of various ratios to obtain uniform spheroids with collagenous regions. PDAC cells were labeled with CellTracker Green™ before being co-cultured with PSCs. After co-culture, we observed pockets of PDAC cells growing with a surrounding PSC component (Figure 1). This feature mimics micro-regions found in common PDAC tumor structure and this co-culture combination is a better 2D model for PDAC than PDAC cells cultured alone. The viability of PANC-1, Capan-1, PSCs when cultured separately in DMEM plus 15% FBS and 1% penicillin for 5 days was 97%, 92% and 94%, respectively, measured via the Trypan Blue assay (Data not shown).

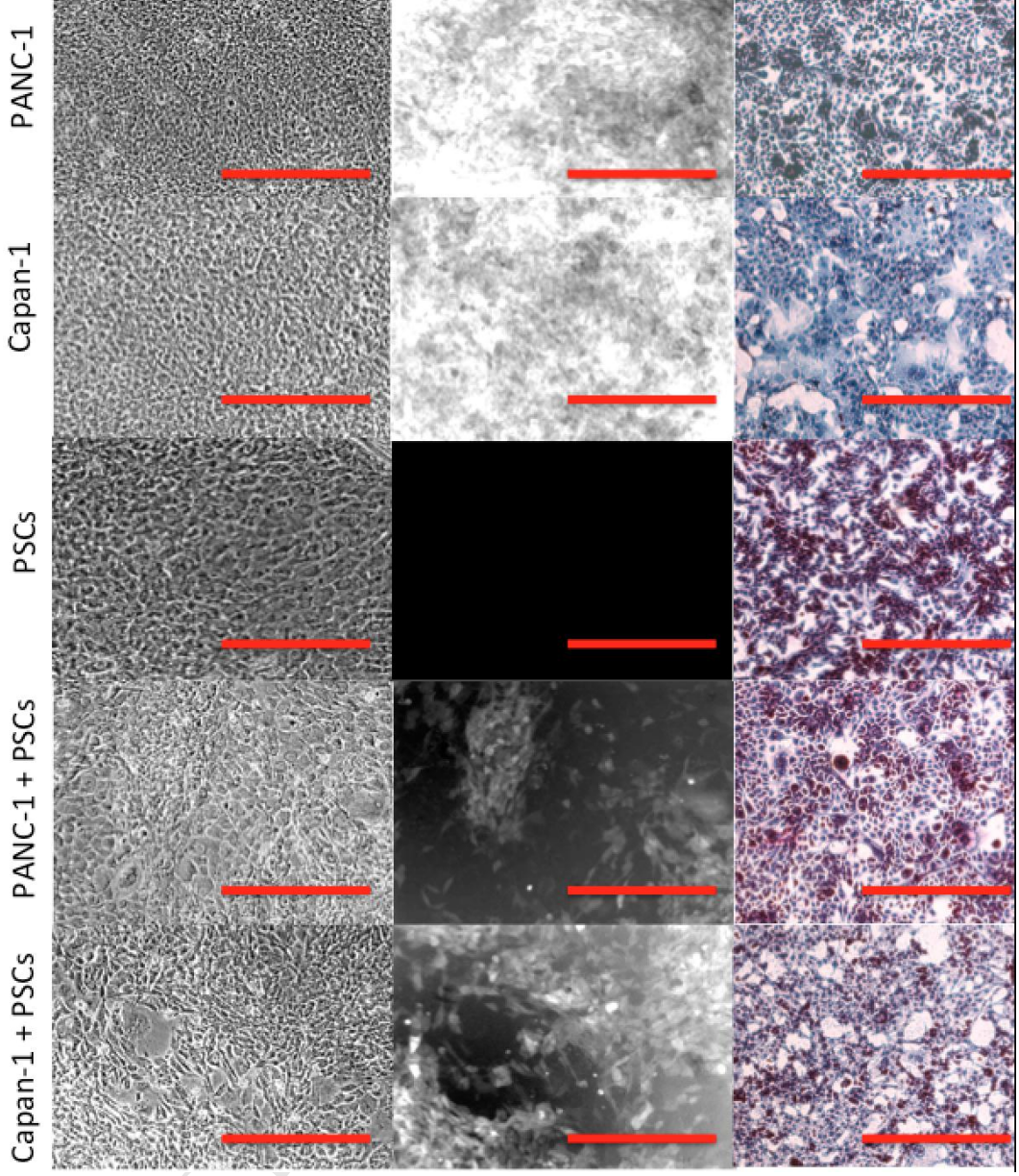

Figure 1: Co-culture of PANC-1 and Capan-1 cells with PSCs in 2-D monolayer settings. PDAC cells were labeled with CellTracker CMFDA Green™ before being co-cultured with unlabeled PSCs. Brightfield, FITC fluorescence and color picro-sirius red images of Panc-1 cells alone, Capan-1 cells alone, PSCs alone, PANC-1 and PSCs (co-cultured in 2:1 ratio) and Capan-1 and PSCs (co-cultured in 2:1 ratio) (Scale bars = 1000μm)

3.2. Proteomic analysis

We utilized the reverse-phase protein assay (RPPA) to identify differentially expressed biomarker proteins when PSCs are co-cultured with PANC-1 or PANC-1 cells are

was used to identify significantly differentiated levels of total or phosphoproteins with p-value < 0.05 and fold-change > 1.25 (or < 1/1.25). In comparison to single medias (PSCs or PANC-1), PSCs co-cultured in PANC-1 resulted in 66 up regulated and 43 down-regulated proteins while PANC-1 cells co-cultured in PSCs resulted in 27 up regulated and 37 down-regulated proteins (Figure 2a, Tables S2a, S2b).

Table S2a and S2b (supplementary) show that p21 is one of the most dramatically up regulated proteins in both sets of cells when exposed to each conditioned media. It has previously been described that p21 can mediate many different cellular processes especially those contributing to cancer development and progression including the interplay with the pancreatic stroma[31]. Laminin5 is also strongly up regulated in both cell lines. Laminins are a family of extracellular matrix glycoproteins and are the major constituents of basement membranes. They have been implicated in a wide variety of biological processes including cell adhesion, differentiation, migration, signaling and metastasis. In addition to Laminin5, Snai2 (slug) was also up regulated in both cell lines. Although limited literature exists regarding its role in PDAC stroma development, the slug gene regulates the actin-bundling protein fascin that is involved in late-stage PanIN and PDAC formation in mice[32]. Fascin appears to promote formation of filopodia and invasive activities of PDAC cells[32]. Its levels in human PDAC correlate with outcomes and time to recurrence, indicating it might be a marker or therapeutic target for PDAC [32].

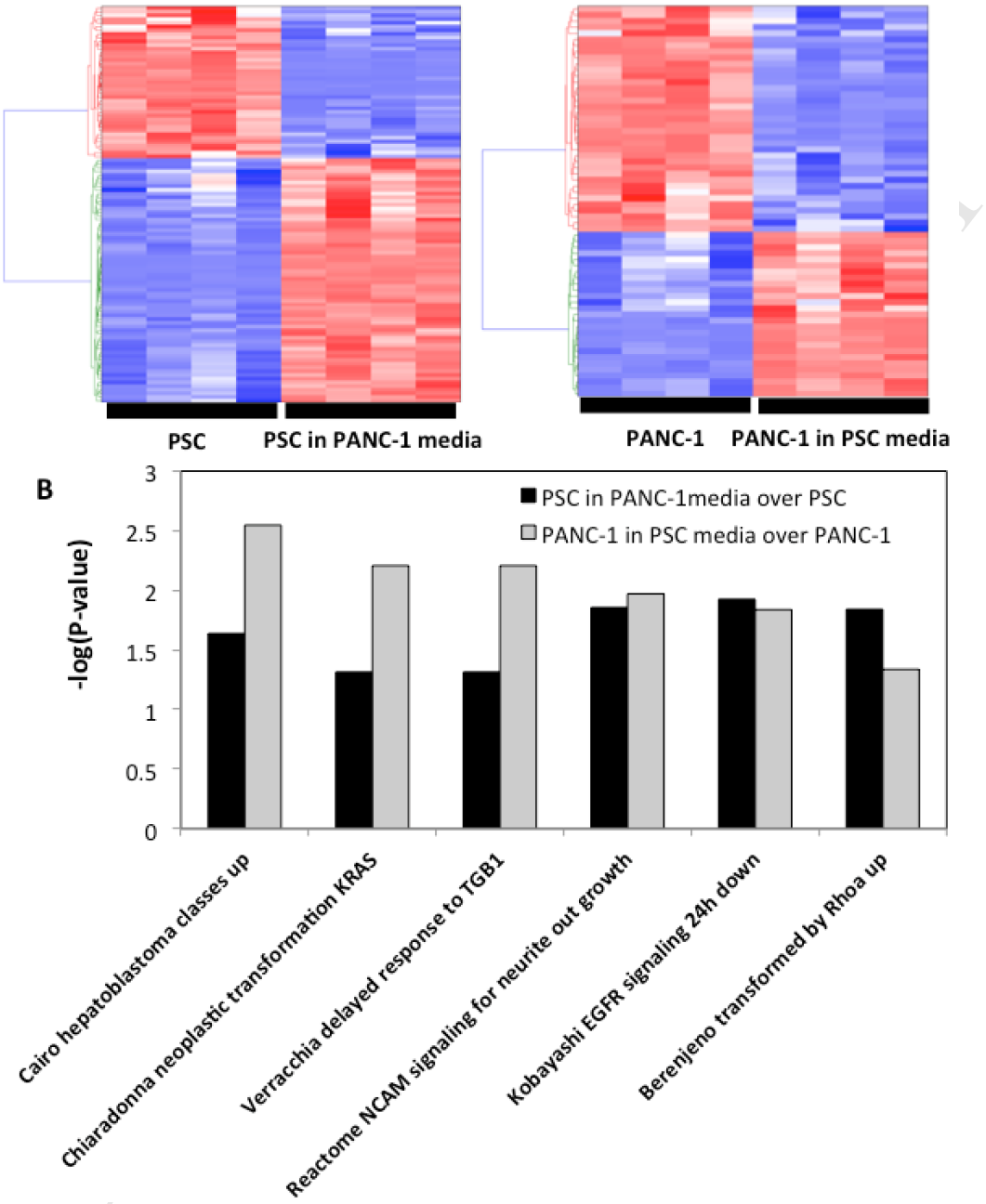

Figure 2: Proteomic analysis of PDAC/PSCs interaction. A) Hierarchical clustering of RPPA data of (left panel) PSC in PANC-1 media versus untreated PCSs and (right panel) PANC-1 in PSC media versus untreated PANC-1 (differentially expressed proteins, t test $P < 0.05$, fold change exceeding 1.25 times). B) Activated stroma related pathways enriched by the core-culture signatures. Data are displayed as the –log of the P value for each pathway.

Catenin (cadherin associated protein) and beta 1 (Ctnnb1) gene (proteins detected by RPPA) are both heavily up regulated by PSCs when cultured with PANC-1 media. These encode an important cytoplasmic component of the classical cadherin adhesion complex that

growth and differentiation during both normal development and tumorigenesis. Analysis of PDAC stroma in comparison to the stroma of chronic pancreatitis also demonstrates overexpression of Wnt5a in PDAC stroma[31]. It has previously been suggested that overexpression of Wnt signaling may contribute to the strong desmoplastic reaction seen in PDAC [33]. The up regulation of MAPK found in this analysis corroborate results from Erkan *et al.*, 2012 who highlighted that activation of stromal cells by pancreatic cancer cells is a persisting event that involves other pathways such as mitogen-activated protein kinase (MAPK)[34] which may lead to the production of dense desmoplastic reaction in PDAC. Both cell lines cultured in conditioned media displayed altered expression of proteins which have previously been shown to be implicated in activated stroma such as integrin, Axl, MMP-9, Stat1, SOCS3 and Vimentin[35]. Gene set enrichment analysis performed using a hyper geometric method revealed that a number of pathways, such as Chiaradonna neoplastic transformation KRAS, Reactome NCAM signaling for neurite out growth and Kobayashi EGFR signaling related to activated stroma[35] are enriched in the co-culture signatures (Figure 2b).

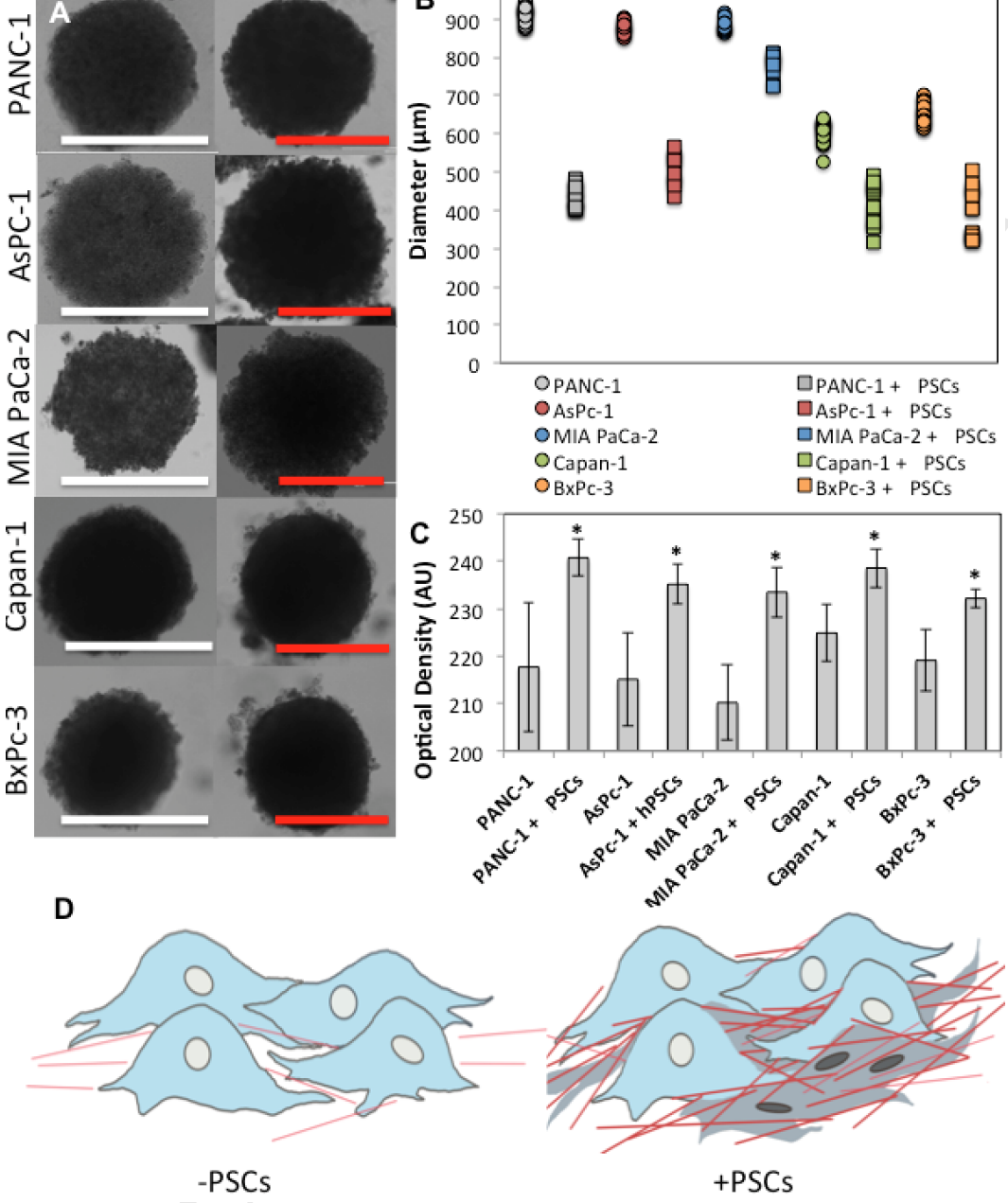

Figure 3: Brightfield microscopy characterization of micro-tumors co-cultured with and without PSCs. A) Brightfield images of PANC-1, AsPc-1, MIA PaCa-2, Capan-1 and BxPc-3 tumors at 7-day time-point. (White scale bar = 1000µm and red scale bar = 500µm m) B) Diameter of PDAC spheroids with and without PSCs at 10-day time-point. C) Optical density of PDAC spheroids with and without PSCs at 10-day time-point ($p<0.01$). D) Schematic representing the increase in density of tumor due to collagen fibers and PSCs packing regions between PDAC cells.

Brightfield microscopy revealed that PDAC-SS were smaller in diameter than their

this phenomenon is that PSCs and their production of ECM proteins, including collagen, create a tightly bound matrix on which the cancer cells grow. Furthermore, collagenous material may fill gaps between the cells to increase density of the overall tumor structure (Figure 3D). The increased density has major implications for the diffusion of drug molecules, and hence may be an important factor in PDAC drug resistance that is commonly observed in human patients.

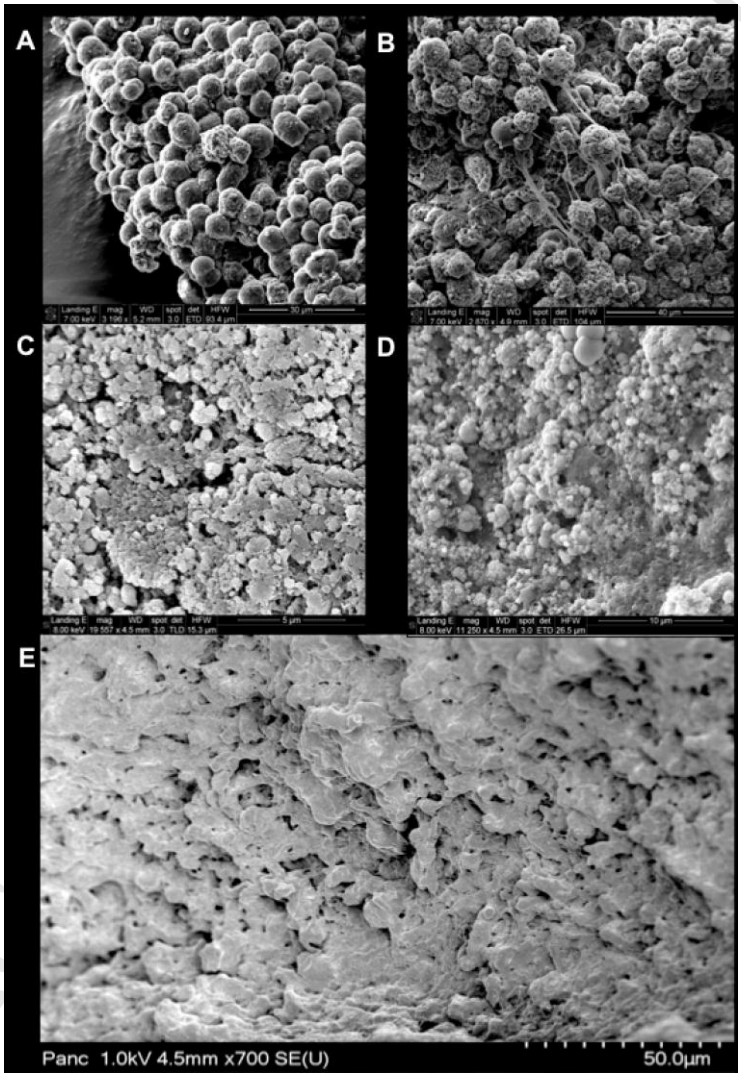

Figure 4: Scanning electron microscopy of tumor surface. Scanning electron micrograph of A) PANC-1 spheroid B) Capan-1 spheroid, C) PANC-1 PDAC-SS, D) Capan-1 PDAC-SS and E) Orthotopic PDAC tumor from mouse model.

Scanning electron micrographs (Figure 4) reveal individual cell aggregates on the

which much more closely resembles the surface of the orthotopic PDAC tumor from a PANC-1 nude mouse model.

3.4 Quantification of collagen content in 3D PDAC-SS

One of the most widely used methods to visualize fibrosis in histological tissue is by staining it with Picro Sirius red [36-40]. Picro Sirius red, in contrast to more traditional stains like van Gieson and trichrome, has greater selectivity and thus is superior for both staining and quantification of collagen [40,41]. Picro Sirius red stains collagenous positive regions within the spheroid red with non-collagenous regions counterstained blue. Figure 5 (and Figure S1) shows extensive Picro Sirius positive regions in PDAC-SS. The percentage area fraction of collagenous regions within each spheroid was calculated based on picro-sirius positive and negative regions. This was also performed on tumor samples that had been generated using PANC-1 and Capan-1 cells injected into the pancreas of nude mice and on human PDAC samples (Figure 4).

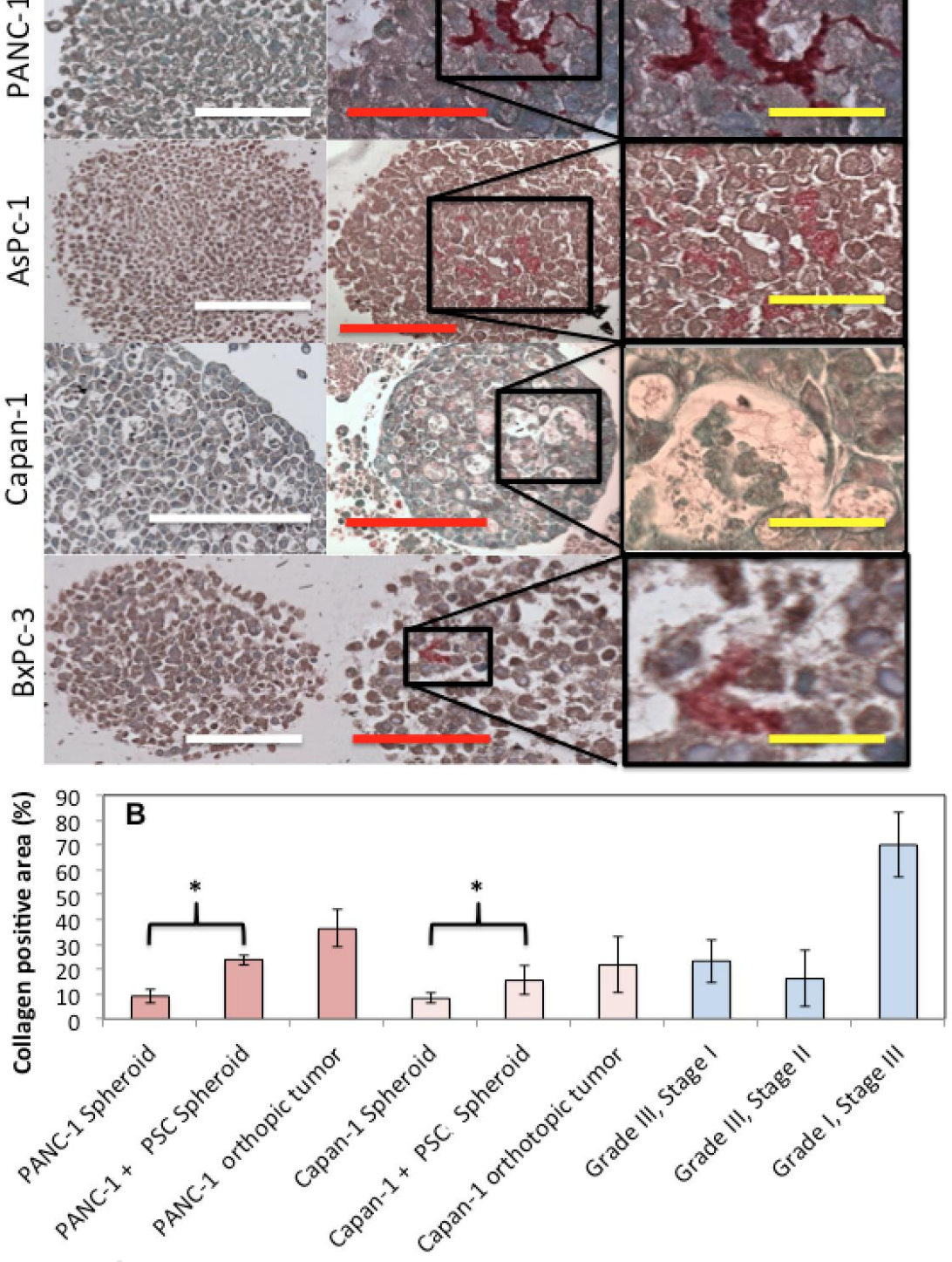

Figure 5: Collagen content of PDAC tumors. A) Picro Sirius staining of various PDAC spheroids with and without PSCs, B) Quantification of collagen positive regions per unit area of tumor. (white and red scale bars= 500μm and yellow scale bars = 200μm *$p<0.05$).

Percentage area fraction of collagen rich was quantified in capan-1 and PANC-1 spheroids due to them being the two most collagenous spheroid models. Limited increases in AsPc-1

2) yielded a 9% and 8% collagen content respectively. PANC-1 and Capan-1 *in vivo* tumors contained 37% and 24% collagen content respectively. This means the spheroids contained more than 4 times less collagen and 3 times less collagen than the *in vivo* tumors. However, PDAC-SS micro-tumors contained 25% (PANC-1) and 18% (Capan-1) collagenous material and hence more accurately represent the amount of collagen found in *in vivo* tumor tissues. Human grade 3 stage 1 and 2 displayed both sparse and dense collagen regions (24% and 18%, respectively) and human grade 1 stage 3 possessed a large amount of sparse and dense collagen (70%).

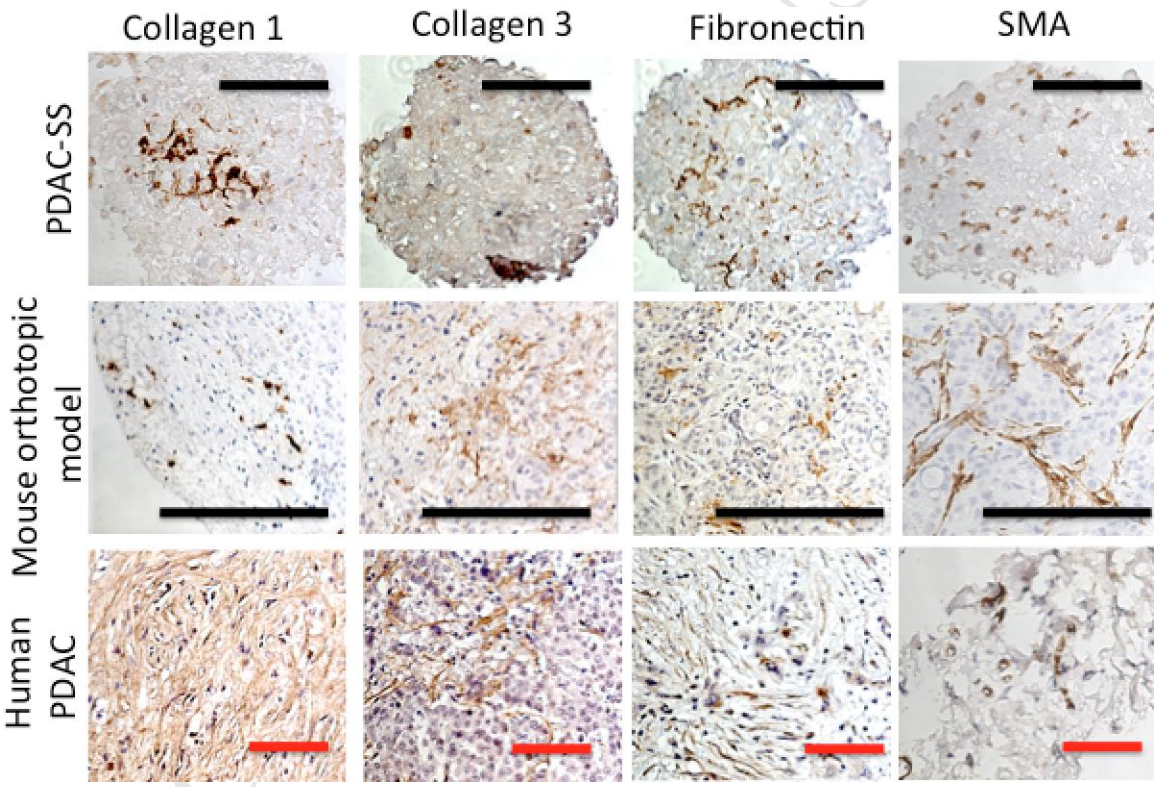

Figure 6: Staining of the stroma fibrosis. Immunohistochemistry of PDAC stroma collagen components in PDAC-SS, as compared to orthotopic PDAC mouse tumors and human grade 2 stage 1 PDAC. Tissues sections stained for collagen 1, collagen 3, and fibronectin and smooth muscle actin (SMA) (Black scale bars = 500μm, red scale bars = 200μm).

3.5 The effect of collagen in PDAC-SS on drug diffusion

Immunohistochemistry determined that the stromal regions in the PDAC-SS model consist

capable of dissipating significant deformation energy [42]. In PDAC, collagen decreases tissue elasticity and increases interstitial pressure, resulting in reduced drug perfusion (Figure 7).

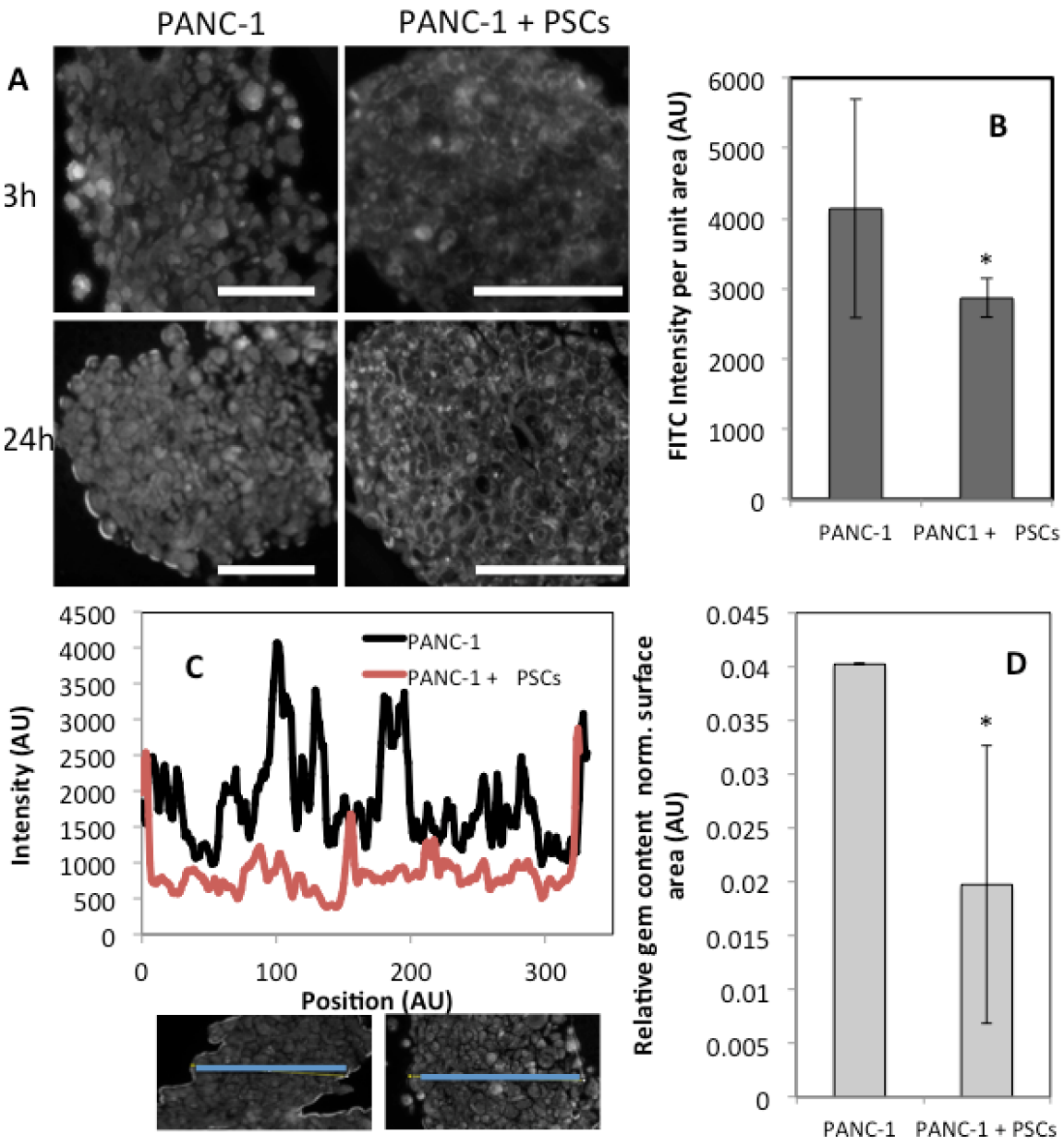

Figure 7: Diffusion of molecules through PANC-1 spheroids with and without PSCs. FITC fluorescent molecule (MW=389.382 g/mol) was used as a model for gemcitabine (MW=263.198 g/mol) to visualize the diffusion through PANC-1 spheroids with and without PSCs. (A) FITC fluorescent images of PANC-1 spheroid regions with and without

from spheroid border through to spheroid centre (lower inlaid images display typical position of intensity measurement across centre of spheroid) D) LC-MS quantification of gemcitabine content normalized to spheroid surface area (spheroid assumed to be perfectly spherical during normalization) in PANC-1 spheroids with and without PSCs (Scale bars = 300μm, * indicates $p<0.05$).

FITC fluorescent marker was used to measure the molecular perfusion (FITC MW 389g/mol, gemcitabine MW=263g/mol) through PDAC spheroids with and without PSCs (Figure 6A-C). LC-MS/MS was also performed to measure the relative gemcitabine content when spheroids with and without PSCs were incubated with 1000uM gemcitabine for 3h. This physiological chemoresistance has previously been shown to be a major contributor to the reduced efficacy of chemotherapeutics in PDAC [43]. As shown in Figure 7, diffusion of both FITC and gemcitabine was significantly impaired in stroma rich spheroids as compared with spheroids composed of only PDAC cells. Figure 8 shows that PDAC-SS model are more structurally viable indicated by the compact nature of the spheroids and have a greater proliferation index (shown by Ki67 expression) after 24h exposure to 1000uM gemcitabine, when compared to spheroids without the PSCs/fibrotic component.

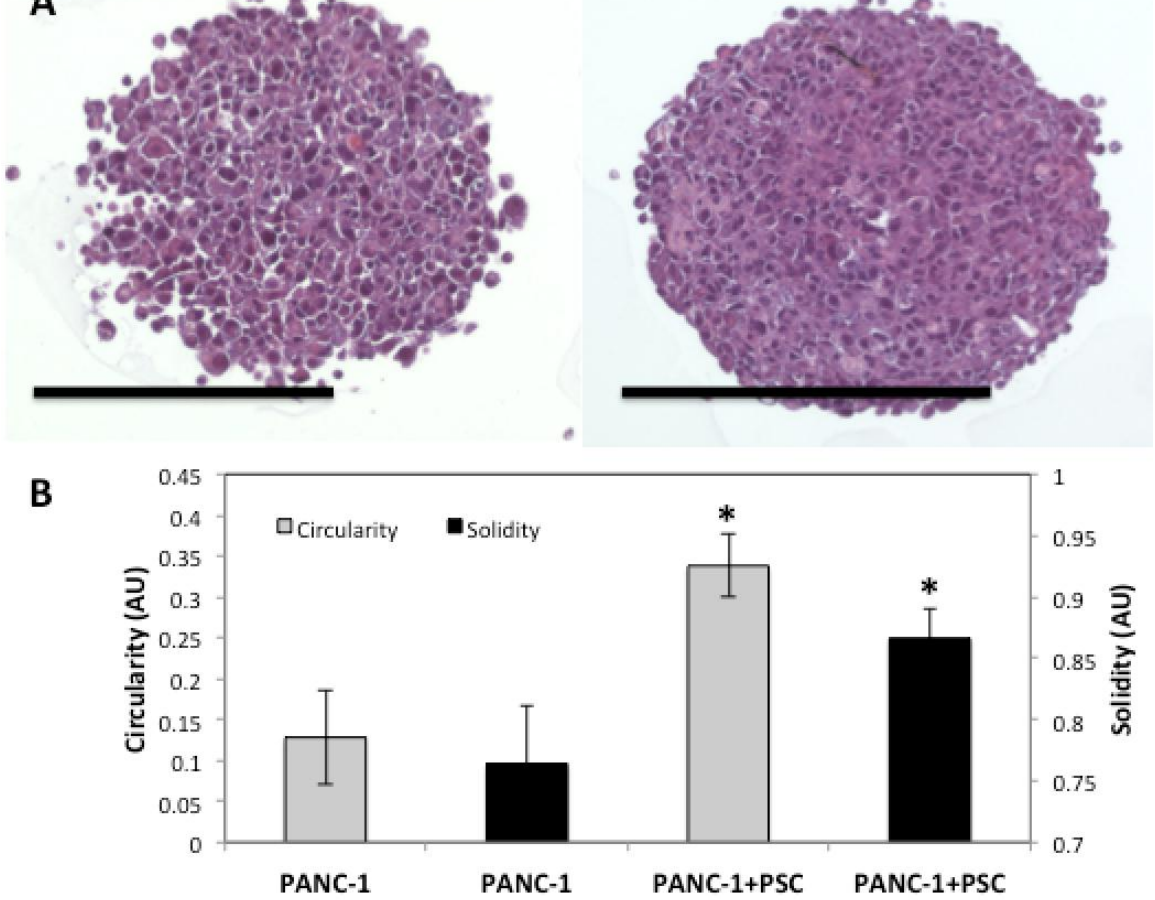

Figure 8: Histological analysis after 24h exposure of gemcitabine. Structural integrity and of PDAC spheroids with and without PSCs after 24h gemcitabine exposure. A) Color images of H&E stained histological slides show (left) zoomed representative image of a PANC1 spheroid without PSCs and (right) a PANC1 spheroid with PSCs after 24h gemcitabine exposure. B) Quantification of circularity and solidity of PANC-1 spheroids with and without PSCs. (scale bars = 1000μm, $p<0.01$) (Robustness of segmentation algorithm is shown in Figure S7). *$p<0.05$.

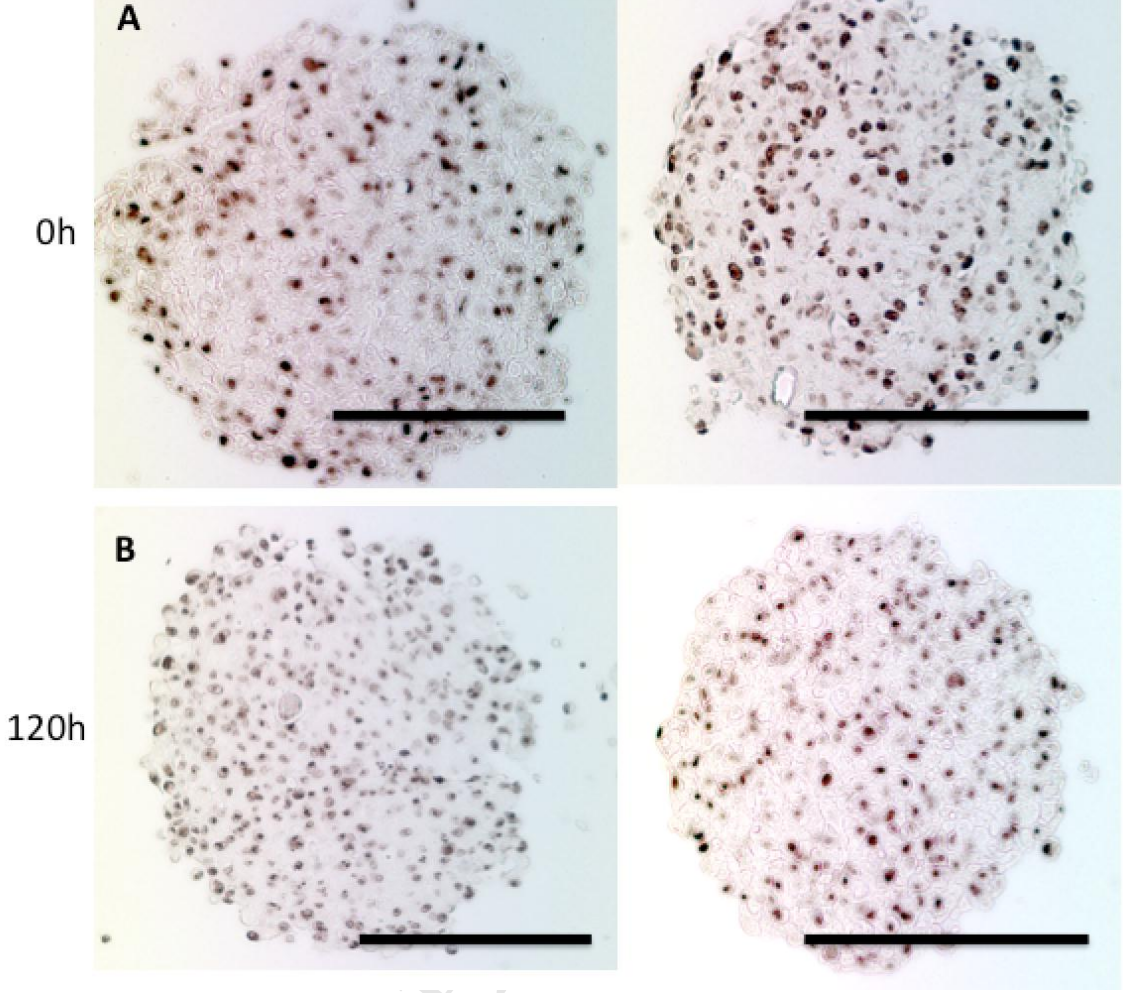

Figure 9: Histological analysis after 120h exposure of gemcitabine. Proliferative index, measured by Ki67 staining, of PDAC spheroids with and without PSCs after 120h gemcitabine exposure. Color images of Ki67 stained histological slides show (left) PANC1 spheroids without PSCs and (right) PANC1 spheroids with PSCs after 0h (top row) and 120h (bottom row) gemcitabine exposure.

PANC1 spheroids with PSCs display a much more dense appearance and increased structural integrity after gemcitabine exposure as given by circularity and solidity measurements. Circularity and Solidity are given by equations 1 and 2 respectively and are shape descriptors used to quantify the structure of the spheroids before after gemcitabine exposure (Figure 8). However, it was also observed that PANC1 spheroids with PSCs displays comparable ki67 content when compared to PANC-1 spheroids without PSCs before and after 120h of gemcitabine exposure (Figure 9).

A key histopathological feature of PDAC that is associated with its innate clinical and biological aggressiveness is its pronounced desmoplastic (stromal) reaction, which is now considered a potential therapeutic target in PDAC [44]. Stroma production is stimulated by cancer-cell derived growth factors including transforming growth factor- β (TGF β), hepatocyte growth factor (HGF), fibroblast growth factor (FGF), insulin-like growth factor 1 (IGF-1) and epidermal growth factor (EGF) [45].The desmoplastic reaction is composed of ECM proteins, primarily type I and III collagen, fibronectin and proteoglycans; small endothelium lined vessels; and a diverse population of cells including inflammatory cells, fibroblasts and stellate cells [46]. The stroma can form up to 90% of the tumor volume, a property which is unique to pancreatic cancer [47,48]. The response of pancreatic cancer cells to chemotherapeutic agents *in vitro* is similar to cell lines derived from other solid tumors [48]. However, pancreatic cancer patients have a limited response to drugs such as paclitaxel compared to breast and prostate cancer patients, suggesting that the unique tumor microenvironment in pancreatic cancer plays a role in chemoresistance [48]. Erkan *et al* [49] observed through staining pancreatic cancer tissue sections of patients for alpha smooth muscle actin (α-SMA the cytoskeletal protein marker for PSC activation) and collagen that a high activated stroma index (α-SMA/collagen) correlated with a poor prognosis. Furthermore, the extensive ECM deposition by PSCs in pancreatic cancer causes distortion and compression of tumor vasculature by fibrous tissue, which contributes to tumor hypoxia, a determinant of chemoresistance [5,50]. Therefore, improved *in vitro* models of PDAC with active stroma, such as our PDAC-SS model, will enhance understanding of the dynamic interaction between cancer cells and stroma compartments. This is an important consideration when designing new, effective therapeutic strategies for pancreatic cancer.

Both PDAC-SS and orthotopic tumors displayed both sparse and dense collagenous areas, indicated by the dim and bright red picro sirius positive regions, respectively. PANC-1 PDAC-SS contained very dense collagen whereas Capan-1 PDAC-SS contained collagen fibers that had shrunk, most probably through histology preparation, to leave blank spaces within the tumor architecture. This feature is also seen in orthotopic tumor collagen. Tumor spheroids grown without PSCs, in contrast, displayed only sparse collagen and notably no dense collagenous areas.

Although the main focus of this work considered stroma content,

the viability of the spheroids at time points passed 2 weeks. However, the time point at harvest was chosen particularly because it represents the time in which the spheroids are most structurally viable. Since stroma rich pancreatic tumors should grow for longer periods of times in vivo (~1-2 months) we will not be able to maintain our spheroids for that long due to obvious limitations of the in vitro cell culture. However, at 7-10 day growth time we have found that the expression of such hallmarks of cancer, which include Ki-67 and HIF-1α is similar between the PDAC-SS and the tumors grown orthotopically in the pancreas of mice. The expression of the human monoclonal Ki-67 antibody is strictly associated with cell proliferation. Ki-67 protein is present during all active phases of the cell (G1, S, G2, and mitotic phases) but is absent from resting cells (G0 phase), which makes it an reliable marker for determining the growth fraction of cells in a given cell population[51]. The fraction of Ki-67-positive tumor cells, also known as the Ki-67 labeling index, is often correlated with the clinical course of the disease[51] Ki-67 has been used in combination with other biomarkers and clinicopathological predictors to predict patient survival post surgery in pancreatic cancer [52].

PDAC-SS also expressed hypoxia-inducible factor 1 alpha, (HIF-1α) which is a transcription factor that mediates cellular and systemic homeostatic responses to reduced O_2 availability in mammals, including angiogenesis, erythropoiesis and glycolysis. HIF-1α is over expressed during carcinogenesis and wound healing. It is crucial for the cellular response to hypoxia and is frequently over expressed in human cancers, resulting in the activation of genes essential for cell survival. HIF-1α regulates the survival and function in the inflammatory microenvironment directly.

Proteomic-based approaches were also used to highlight potential genes, some of which are already known to be associated with PDAC-stroma interactions and fibrosis development in PDAC and some of which are not currently known. With a recent interest in moving toward an integrative, rather than reductionist, approach to PDAC biology in the post-genomic era, proteomic pattern comparisons between 2D and 3D mono and co-cultures may lead to the discovery of numerous potential biomarkers that could be translated into diagnosis or prognosis in the clinical field.

Finally, we demonstrated that the PDAC-SS model displayed a lower molecular perfusion and a slight trend in higher proliferative index after 24h exposure of FITC

gemcitabine. In in-vivo scenarios, 30-60mg/kg may be injected into the mouse with a fraction of this dose arriving at the tumor. This model can act as a bridge between in vitro and in vivo as in vitro doses are used however not all cells posses a cell-drug interface which is comparable to in vivo situation.

5.0 Conclusions

It is clear that the prominent stromal/desmoplastic reaction of PDAC can no longer be dismissed as a mere epiphenomenon of carcinogenesis. Indeed, available evidence strongly indicates that this stromal reaction, and in particular the cells responsible for its production, PSCs, likely play a key role at the different stages of pancreatic cancer development and response to therapy. Therefore, all components of this reaction (stromal cells and collagenous matrix) warrant attention as potentially useful, additional therapeutic targets in this disease. In this work, we have developed an *in vitro* model of PDAC tumor that incorporates a prominent desmoplastic reaction through the incorporation of PSCs into a spheroid model. Spheroids grown with PSCs are more dense and compact and exhibit larger collagen content than spheroids grown solely with PDAC cell lines. In addition to similarities in collagen content, PDAC-SS are also very similar to orthotopic tumors in expression of KI67 and HIF-1α. PDAC-SS are thus an important advancement in the development of in vitro tumor models that closely resemble actual tumor microenvironments in patients. Future challenges in this field of research will be to develop experimental 3D *in vitro* models (or a range of models) that not only closely simulate the pathology, but also account for the heterogeneity and full range of cell types found in human PDAC, so as to successfully translate research findings into clinically effective therapies.

Acknowledgments

B.G. acknowledges the financial support from NIH U54CA143837 Physical Sciences and Oncology grant, NIH 1U54CA151668-01 Cancer Centre for Nanotechnology Excellence grant and 1R21HD082947. MJW, SC and SJC acknowledge the financial support from Kanzius Cancer Research Foundation. The authors would also like to acknowledge kind assistance of Kemi Cui (HMRI Advanced Cellular and Tissue Microscope Core Facility) for his help with acquiring color histological images. SH, CC and KR acknowledges the financial

Grant to Antibody-based Proteomics Core/Shared Resource (P30CA125123) (DPE and SH). The metabolomics core is also supported by CPRIT Core facility award RP120092-DPE is PI). The authors would also like to acknowledge the LC-MS/MS work performed by Sri Ramya Donepudi and Nagireddy Putluri in Advanced Technology Core, Baylor College of Medicine. The Advanced Technology Core is supported by the following grants: NCI/ 2P30CA125123-09 Shared Resources Metabolomics core and funds from Dan L. Duncan Cancer Center (DLDCC), Baylor college of Medicine.

Author Contributions

The study was conceived by M.J.W., B.G., S.J.C. and S.A.C. M.W. and B.G. designed the experiments. M.W., J.L., V.K., J.C.H and C.A.F. performed the experiments. B.S. and S.M. performed histology. P.R. provided MATLAB analysis code. S.H., K.R. and C.C. performed the RPPA and provided statistics on proteomic data. The manuscript was written by M.J.W. and BG and edited by all authors before submission. R.H. provided the PSCs.

5.0 Supplementary Section

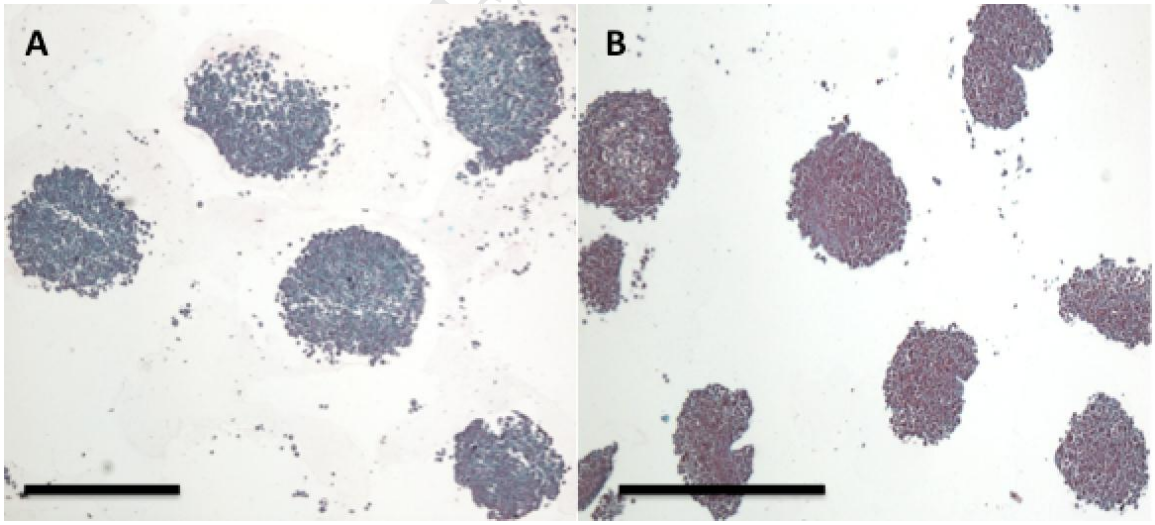

Figure S1: Wide angle (x4) image of PANC-1 spheroids staining of picro sirius showing redness (collagen positive) of spheroids (A) without PSCs and (B) with PSCs.

The MATLAB algorithm created to segment and count the number of red pixels within an image

```
% %cd('C:\Users/matthewware/Desktop/');% specifies the directory or
folder the image is located

clear;
cd('/Users/matthewware/Desktop/');% specifies the directory or folder
the image is located
img=imread('tile_x007_y001.tif'); %imports the image by image name

red = img(:,:,1); % Red channel
green = img(:,:,2); % Green channel
blue = img(:,:,3); % Blue channel

red_dots = (red(:,:)>5& green(:,:)<115 & blue(:,:)<115);

figure, imshow(img), title('Original image')
figure, imshow(red), title('Red channel')
figure, imshow(redish_dots), title('Red pixels')

sum(red_dots(:))
```

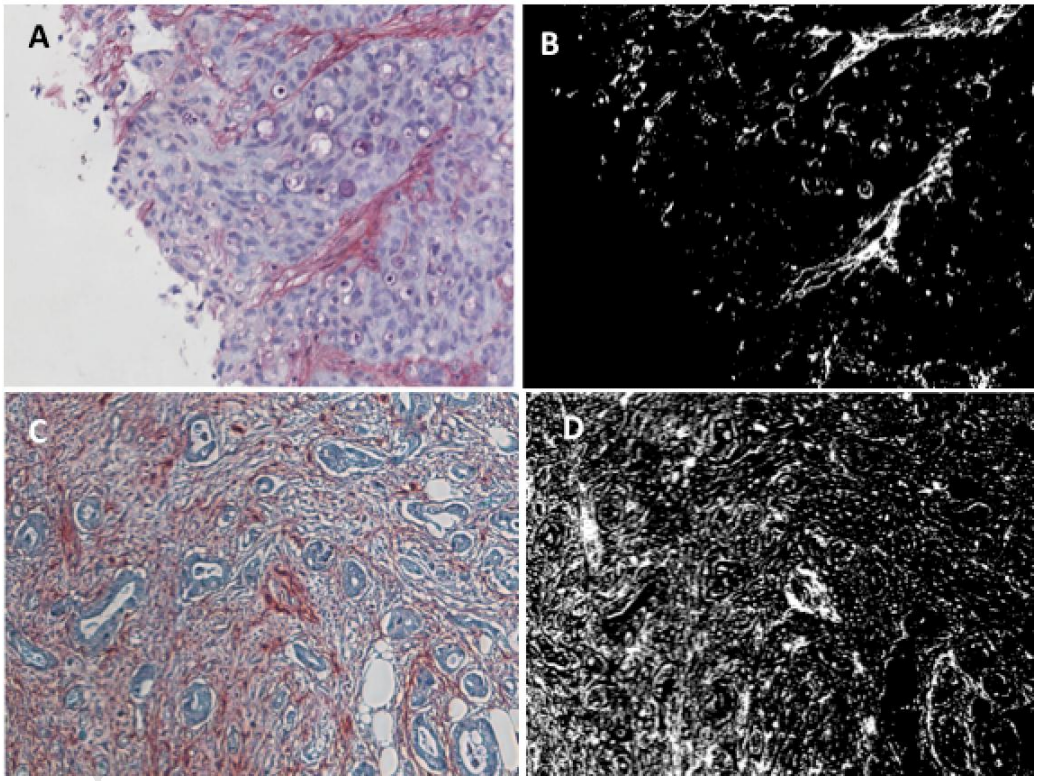

Figure S2: Collagen content quantification algorithm. Collagen content was calculated via a MATLAB generated algorithm. A) Raw RGB color image before processing and B) binary image after processing (picro-sirius regions represented by white pixels) of Orthotopic tumor from mouse model. C) Raw RGB color image before processing and B) binary image after processing of human grade 1, stage 1 PDAC tumor.

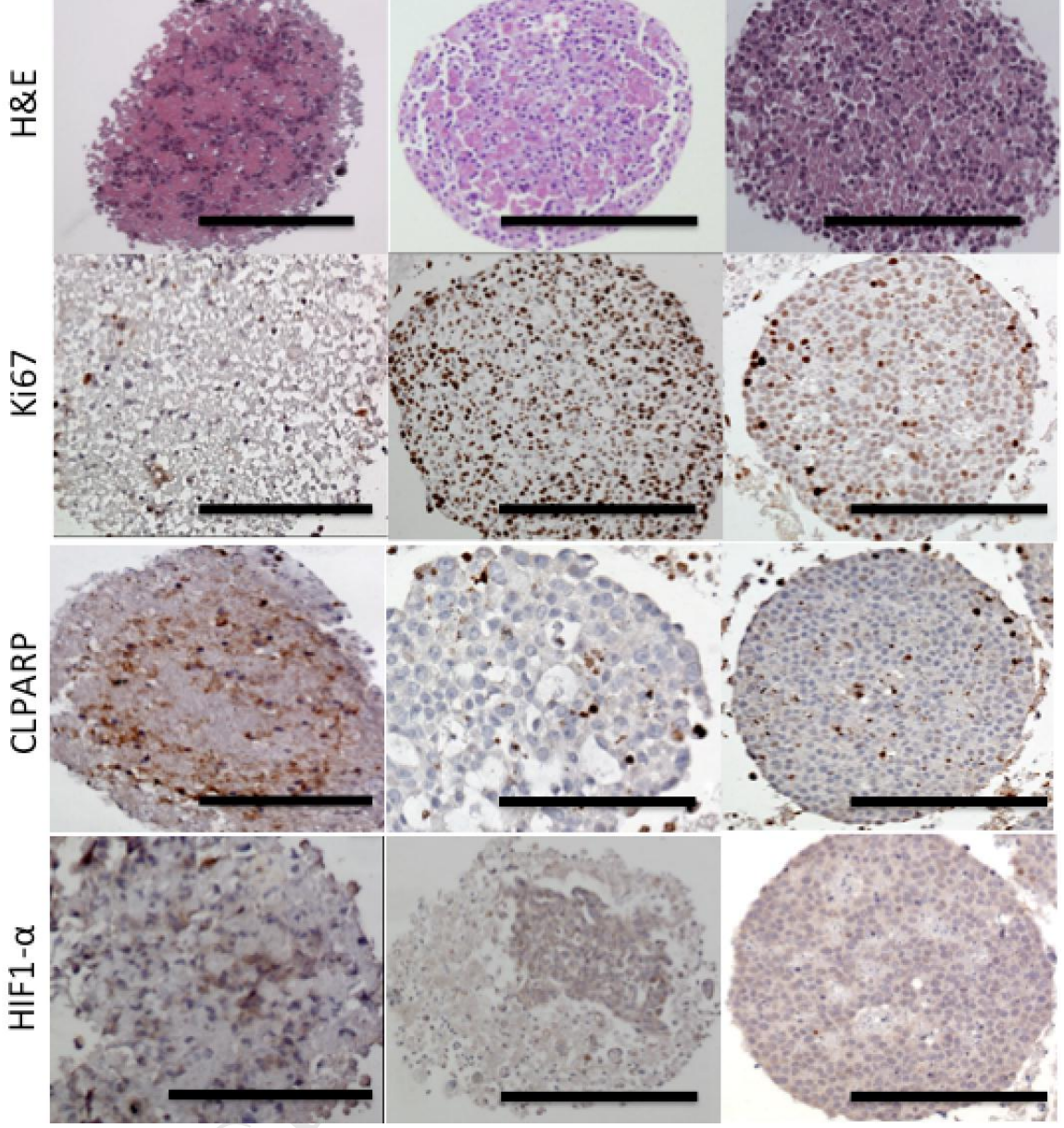

Figure S3: Histological analysis of tumor spheroids generated without PSCs. PANC-1, Capan-1 and BxPc-3 cells grown in our new hanging drop method for 10 days before histological analysis, including H&E, Ki67 (proliferation), CLPARP (apoptosis) and Hif 1-α (hypoxia) (Scale bars = 500μm).

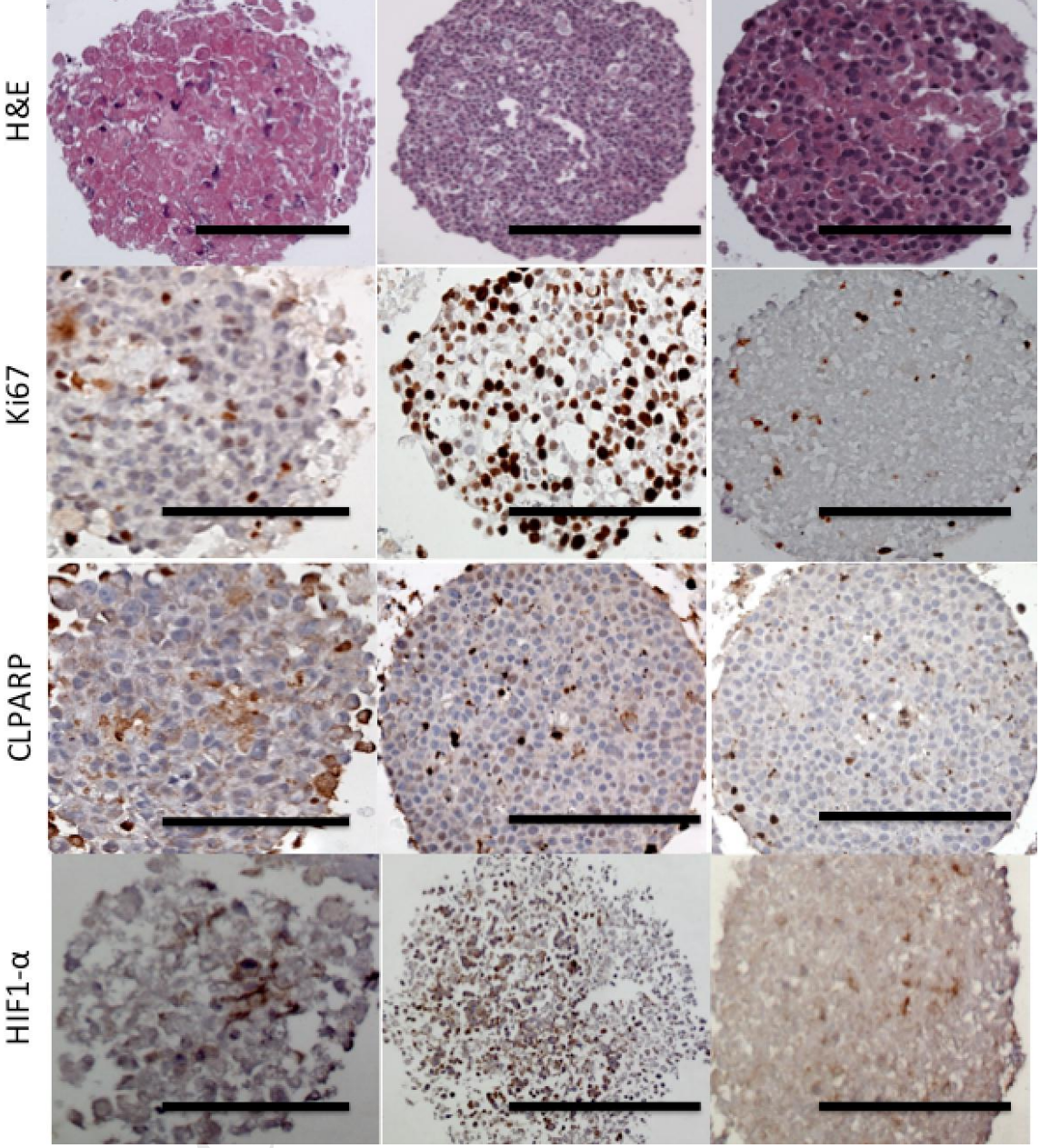

Figure S4: Histological analysis of micro-tumors generated with PSCs. PANC-1, Capan-1 and BxPc-3 cells grown in our new hanging drop method for 10 days before histological analysis, including H&E, Ki67 (proliferation), CLPARP (apoptosis) and HIF 1-α (hypoxia).

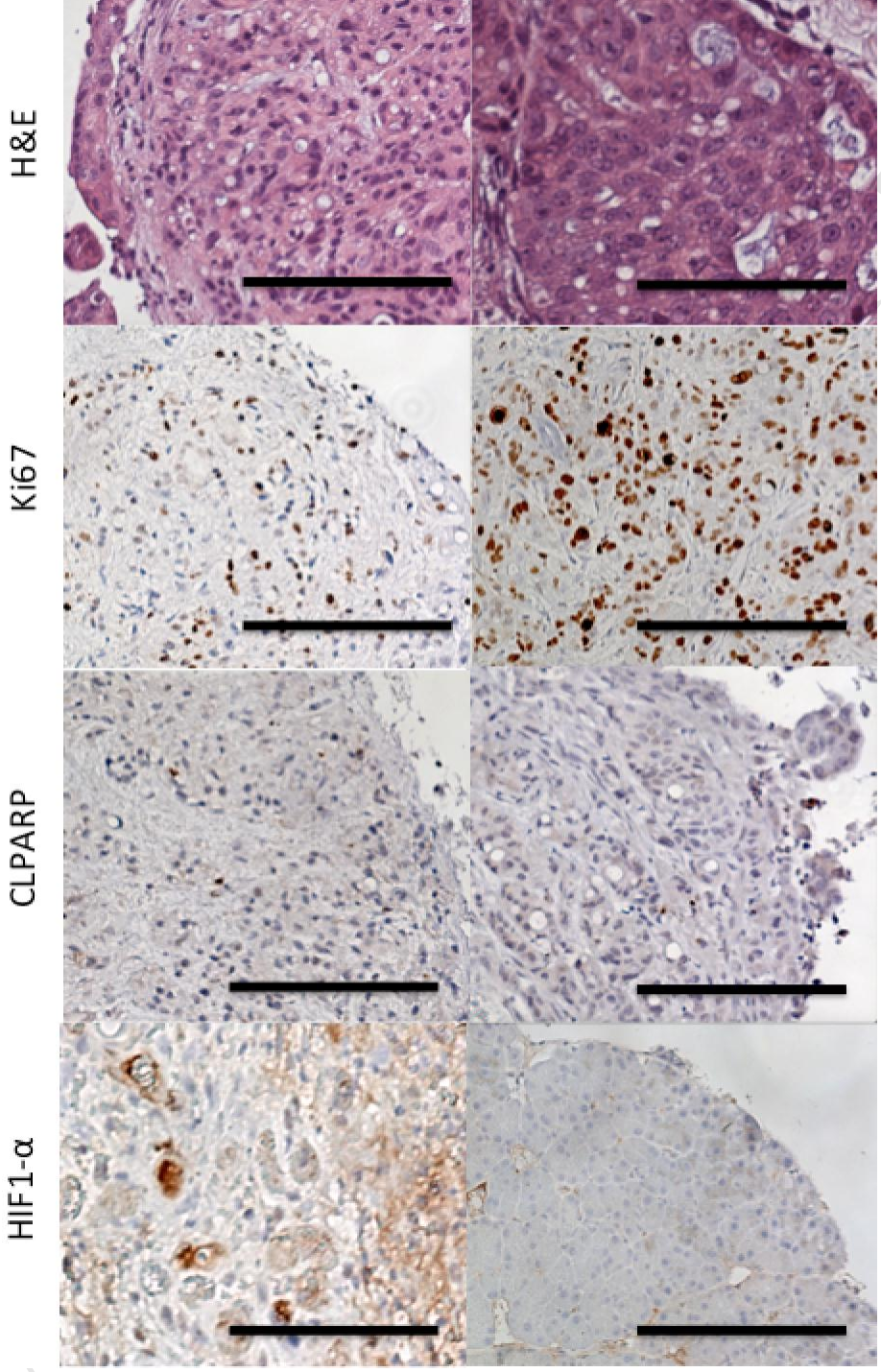

Figure S5: Histological analysis of PDAC orthotopic mouse tumors. Histological analysis of Panc-1 and Capan-1 orthotopic pancreatic mouse tumors, which includes H&E, Ki67, CLPARP and Hif 1-α (scale bars = 1000μm).

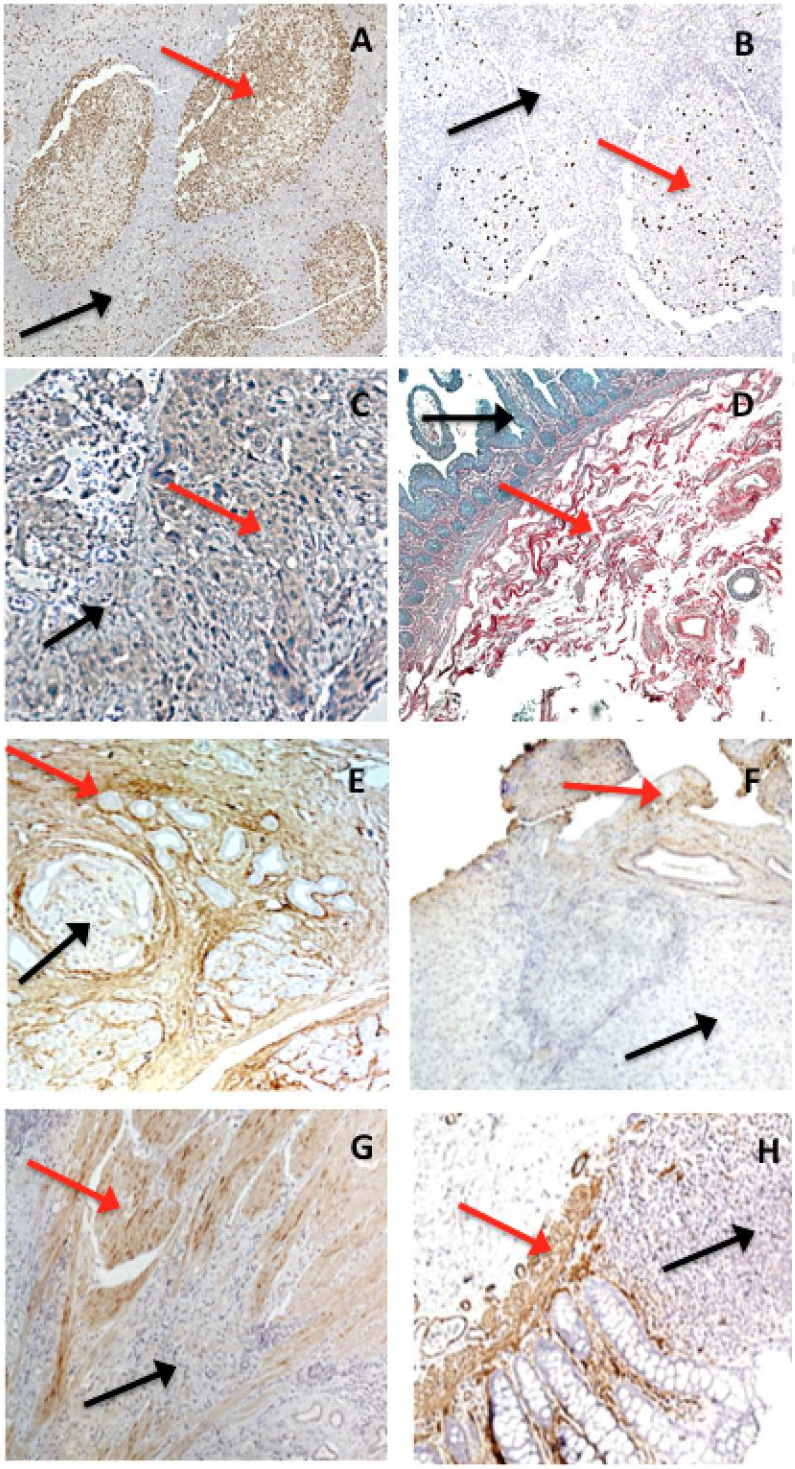

Figure S6: Immunohistochemistry positive staining controls. A) Ki67, B) CLPARP, C) Hif 1-α, D) Picro Sirius, E) Collagen 1, F) Collagen 3, G) Fibronectin and H) SMA. Red and black arrows indicate positively and negatively stained regions, respectively.

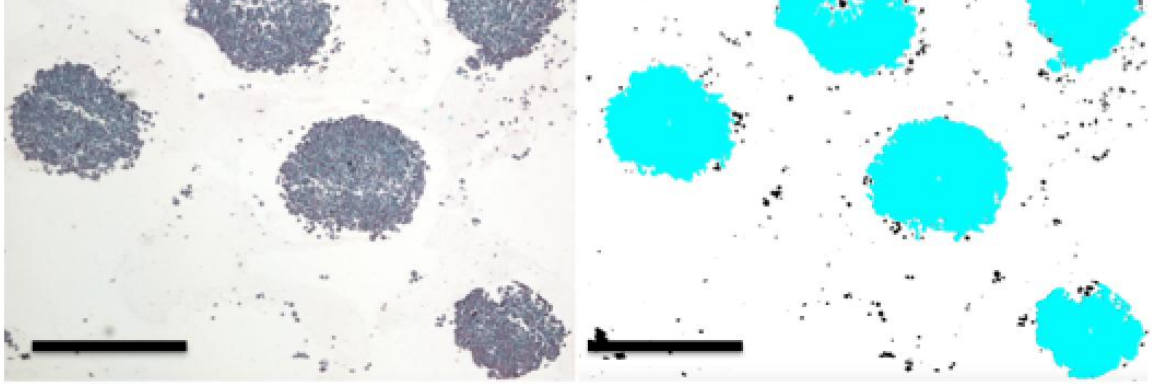

Figure S7: Robustness of segmentation algorithm for shape descriptor analysis. A) Raw color image and B) Binary transformed image with segmentation (Scale bars = 1000μM).

Table S2a: Altered gene expression in PSC cells cultured in PDAC conditioned media.

Altered genes in PSCs when cultured in PDAC conditioned media (Gene symbol)	Relative effect (Z-score, + denotes up-regulation and – denotes down regulation)	*p-value*
CDKN1A	+2.85	2E-09
LAMC2	+2.76	2E-09
SNAI2	+2.53	2E-10
MAP1LC3B	+1.96	2E-09
CTNNB1	+1.89	2E-08
CDH1	+1.71	2E-06
CDKN1B	+1.62	4E-08
AKT1, AKT2, AKT3	+1.61	2E-07
PTK2	+1.54	1E-06
YWHAZ	+1.43	1E-04
SRC	+1.21	2E-05
ITGB3	+1.2	3E-04
PRKAA1	+1.19	2E-08
MAPK1, MAPK3	+1.16	2E-05
SHC1	+1.12	1E-08
MAP1LC3A	+1.07	4E-05
FGFR1	+1.05	2E-05
FOS	-3.77	2E-10
CHAF1A	-3.55	7E-10
MKI67	-3.25	4E-09
RRM2	-3.18	3E-09
AURKA, AURKB, AURKC	-2.27	2E-07
PRKAA1, PRKAA2	-2.11	2E-09
RB1	-2.09	2E-07

STAT1	-1.26	6E-07
LRP6	-1.21	9E-06
ERBB3	-1.13	1E-05
VIM	-1.09	5E-05
SOCS3	-1	5E-05

Table S2b: Altered gene expression in PDAC cells cultured in PSCs conditioned media.

Altered genes in PDAC cells when cultured in PSC conditioned media (Gene symbol)	Relative effect (Z-score, + denotes up-regulation and – denotes down regulation)	*p-value*
SNAI2	+2.49	1.1E-08
CDKN1A	+1.98	1.4E-07
LAMC2	+1.87	1.3E-08
ITGB3	+1.86	9.2E-04
PTK2	+1.19	4.4E-07
YWHAZ	+1.18	4.8E-05
MAP1LC3B	+1.07	4.4E-08
MKI67	-1.99	1.61E-08
ERBB3	-1.55	1.22E-06
FOS	-1.44	1.37E-06
CHAF1A	-1.38	4.24E-07
VIM	-1.22	1.09E-05
CASP7	-1.05	1.80E-05

1 Jemal, A. *et al.* Global cancer statistics. *CA: a cancer journal for clinicians* **61**, 69-90, doi:10.3322/caac.20107 (2011).
2 Siegel, R., Naishadham, D. & Jemal, A. Cancer statistics, 2013. *CA: a cancer journal for clinicians* **63**, 11-30, doi:10.3322/caac.21166 (2013).
3 Mantoni, T. S., Lunardi, S., Al-Assar, O., Masamune, A. & Brunner, T. B. Pancreatic stellate cells radioprotect pancreatic cancer cells through beta1-integrin signaling. *Cancer research* **71**, 3453-3458, doi:10.1158/0008-5472.can-10-1633 (2011).
4 Trouilloud, I. *et al.* Medical treatment of pancreatic cancer: new hopes after 10 years of gemcitabine. *Clin Res Hepatol Gastroenterol* **35**, 364-374, doi:10.1016/j.clinre.2011.02.002 (2011).
5 Olive, K. P. *et al.* Inhibition of Hedgehog signaling enhances delivery of chemotherapy in a mouse model of pancreatic cancer. *Science* **324**, 1457-1461, doi:1171362 [pii]
10.1126/science.1171362 (2009).
6 Apte, M. V. *et al.* Periacinar stellate shaped cells in rat pancreas: identification, isolation, and culture. *Gut* **43**, 128-133 (1998).
7 Tahara, J., Shimizu, K. & Shiratori, K. Engulfment of necrotic acinar cells by pancreatic stellate cells inhibits pancreatic fibrogenesis. *Pancreas* **37**, 69-74, doi:10.1097/MPA.0b013e318160a5cb (2008).
8 Apte, M. V. *et al.* Desmoplastic reaction in pancreatic cancer: role of pancreatic stellate cells. *Pancreas* **29**, 179-187 (2004).
9 Xu, Z. *et al.* Role of pancreatic stellate cells in pancreatic cancer metastasis. *The American journal of pathology* **177**, 2585-2596, doi:10.2353/ajpath.2010.090899 (2010).
10 Wilson, J. S., Pirola, R. C. & Apte, M. V. Stars and stripes in pancreatic cancer: role of stellate cells and stroma in cancer progression. *Frontiers in physiology* **5**, 52, doi:10.3389/fphys.2014.00052 (2014).
11 Tang, D. *et al.* High expression of Galectin-1 in pancreatic stellate cells plays a role in the development and maintenance of an immunosuppressive microenvironment in pancreatic cancer. *International journal of cancer. Journal international du cancer* **130**, 2337-2348, doi:10.1002/ijc.26290 (2012).
12 Ene-Obong, A. *et al.* Activated pancreatic stellate cells sequester CD8+ T cells to reduce their infiltration of the juxtatumoral compartment of pancreatic ductal adenocarcinoma. *Gastroenterology* **145**, 1121-1132, doi:10.1053/j.gastro.2013.07.025 (2013).
13 Hwang, R. F. *et al.* Cancer-Associated Stromal Fibroblasts Promote Pancreatic Tumor Progression. *Cancer research* **68**, 918-926, doi:10.1158/0008-5472.CAN-07-5714 (2008).
14 Mellor, H. R., Ferguson, D. J. & Callaghan, R. A model of quiescent tumour microregions for evaluating multicellular resistance to chemotherapeutic drugs. *British journal of cancer* **93**, 302-309, doi:10.1038/sj.bjc.6602710 (2005).

Journal of biomolecular screening **9**, 273-285, doi:10.1177/1087057104265040 (2004).

16 Hicks, K. O., Pruijn, F. B., Sturman, J. R., Denny, W. A. & Wilson, W. R. Multicellular resistance to tirapazamine is due to restricted extravascular transport: a pharmacokinetic/pharmacodynamic study in HT29 multicellular layer cultures. *Cancer research* **63**, 5970-5977 (2003).

17 Ijichi, H. Genetically-engineered mouse models for pancreatic cancer: Advances and current limitations. *World Journal of Clinical Oncology* **2**, 195-202, doi:10.5306/wjco.v2.i5.195 (2011).

18 Waghray, M., Yalamanchili, M., di Magliano, M. P. & Simeone, D. M. Deciphering the Role of Stroma in Pancreatic Cancer. *Current opinion in gastroenterology* **29**, 537-543, doi:10.1097/MOG.0b013e328363affe (2013).

19 Carapuca, E. F. *et al.* Anti-stromal treatment together with chemotherapy targets multiple signalling pathways in pancreatic adenocarcinoma. *The Journal of pathology*, doi:10.1002/path.4727 (2016).

20 Coleman, S. J. *et al.* Pancreatic cancer organotypics: High throughput, preclinical models for pharmacological agent evaluation. *World journal of gastroenterology* **20**, 8471-8481, doi:10.3748/wjg.v20.i26.8471 (2014).

21 Ware, M. *et al.* Generation of homogenous 3D pancreatic cancer cell spheroids using an improved hanging drop technique *Tissue Engineering C (under review)* (2015).

22 Bachem, M. G. *et al.* Pancreatic carcinoma cells induce fibrosis by stimulating proliferation and matrix synthesis of stellate cells. *Gastroenterology* **128**, 907-921 (2005).

23 Erkan, M. *et al.* Preoperative acute pancreatitis in periampullary tumors: implications for surgical management. *Digestion* **75**, 165-171, doi:10.1159/000106799 (2007).

24 Lieber, M., Mazzetta, J., Nelson-Rees, W., Kaplan, M. & Todaro, G. Establishment of a continuous tumor-cell line (panc-1) from a human carcinoma of the exocrine pancreas. *International journal of cancer. Journal international du cancer* **15**, 741-747 (1975).

25 Chen, W. H. *et al.* Human pancreatic adenocarcinoma: in vitro and in vivo morphology of a new tumor line established from ascites. *In vitro* **18**, 24-34 (1982).

26 Yunis, A. A., Arimura, G. K. & Russin, D. J. Human pancreatic carcinoma (MIA PaCa-2) in continuous culture: sensitivity to asparaginase. *International journal of cancer. Journal international du cancer* **19**, 128-135 (1977).

27 Kyriazis, A. P. *et al.* Human pancreatic adenocarcinoma line Capan-1 in tissue culture and the nude mouse: morphologic, biologic, and biochemical characteristics. *The American journal of pathology* **106**, 250-260 (1982).

28 Tan, M. H. *et al.* Characterization of a new primary human pancreatic tumor line. *Cancer investigation* **4**, 15-23 (1986).

29 Holdman, X. B. *et al.* Upregulation of EGFR signaling is correlated with tumor stroma remodeling and tumor recurrence in FGFR1-driven breast cancer. *Breast Cancer Res* **17**, 141, doi:10.1186/s13058-015-0649-1 (2015).

doi:10.1038/ncb3355 (2016).
31 Pilarsky, C. *et al.* Activation of Wnt signalling in stroma from pancreatic cancer identified by gene expression profiling. *Journal of cellular and molecular medicine* **12**, 2823-2835, doi:10.1111/j.1582-4934.2008.00289.x (2008).
32 Li, A. *et al.* Fascin Is Regulated by Slug, Promotes Progression of Pancreatic Cancer in Mice, and Is Associated With Patient Outcomes. *Gastroenterology* **146**, 1386-1396.e1317, doi:10.1053/j.gastro.2014.01.046 (2014).
33 Pilarsky, C. *et al.* Activation of Wnt signalling in stroma from pancreatic cancer identified by gene expression profiling. *Journal of cellular and molecular medicine* **12**, 2823-2835, doi:10.1111/j.1582-4934.2008.00289.x (2008).
34 Erkan, M. *et al.* The role of stroma in pancreatic cancer: diagnostic and therapeutic implications. *Nature reviews. Gastroenterology & hepatology* **9**, 454-467, doi:10.1038/nrgastro.2012.115 (2012).
35 Moffitt, R. A. *et al.* Virtual microdissection identifies distinct tumor- and stroma-specific subtypes of pancreatic ductal adenocarcinoma. *Nature genetics* **47**, 1168-1178, doi:10.1038/ng.3398 (2015).
36 Junqueira, L. C., Bignolas, G. & Brentani, R. R. Picrosirius staining plus polarization microscopy, a specific method for collagen detection in tissue sections. *The Histochemical journal* **11**, 447-455 (1979).
37 Mito, S. *et al.* Myocardial protection against pressure overload in mice lacking Bach1, a transcriptional repressor of heme oxygenase-1. *Hypertension* **51**, 1570-1577, doi:10.1161/hypertensionaha.107.102566 (2008).
38 Puchtler, H., Waldrop, F. S. & Valentine, L. S. Polarization microscopic studies of connective tissue stained with picro-sirius red FBA. *Beitrage zur Pathologie* **150**, 174-187 (1973).
39 Seeland, U. *et al.* Interstitial remodeling in beta1-adrenergic receptor transgenic mice. *Basic research in cardiology* **102**, 183-193, doi:10.1007/s00395-006-0635-y (2007).
40 Whittaker, P., Kloner, R. A., Boughner, D. R. & Pickering, J. G. Quantitative assessment of myocardial collagen with picrosirius red staining and circularly polarized light. *Basic research in cardiology* **89**, 397-410 (1994).
41 Whittaker, P., Boughner, D. R. & Kloner, R. A. Analysis of healing after myocardial infarction using polarized light microscopy. *The American journal of pathology* **134**, 879-893 (1989).
42 Buehler, M. J. Nature designs tough collagen: explaining the nanostructure of collagen fibrils. *Proceedings of the National Academy of Sciences of the United States of America* **103**, 12285-12290, doi:10.1073/pnas.0603216103 (2006).
43 Heldin, C. H., Rubin, K., Pietras, K. & Ostman, A. High interstitial fluid pressure - an obstacle in cancer therapy. *Nature reviews. Cancer* **4**, 806-813, doi:10.1038/nrc1456 (2004).
44 Kong, X., Li, L., Li, Z. & Xie, K. Targeted Disruption of Orchestration between Stroma and Tumor Cells in Pancreatic Cancer: Molecular Basis and

45 Mahadevan, D. & Von Hoff, D. D. Tumor-stroma interactions in pancreatic ductal adenocarcinoma. *Molecular cancer therapeutics* **6**, 1186-1197, doi:10.1158/1535-7163.mct-06-0686 (2007).
46 Erkan, M., Reiser-Erkan, C., Michalski, C. W. & Kleeff, J. Tumor microenvironment and progression of pancreatic cancer. *Experimental oncology* **32**, 128-131 (2010).
47 Neesse, A. *et al.* Stromal biology and therapy in pancreatic cancer. *Gut* **60**, 861-868, doi:10.1136/gut.2010.226092 (2011).
48 Li, J., Wientjes, M. G. & Au, J. L. Pancreatic cancer: pathobiology, treatment options, and drug delivery. *The AAPS journal* **12**, 223-232, doi:10.1208/s12248-010-9181-5 (2010).
49 Erkan, M. *et al.* The activated stroma index is a novel and independent prognostic marker in pancreatic ductal adenocarcinoma. *Clinical gastroenterology and hepatology : the official clinical practice journal of the American Gastroenterological Association* **6**, 1155-1161, doi:10.1016/j.cgh.2008.05.006 (2008).
50 Couvelard, A. *et al.* Expression of hypoxia-inducible factors is correlated with the presence of a fibrotic focus and angiogenesis in pancreatic ductal adenocarcinomas. *Histopathology* **46**, 668-676, doi:10.1111/j.1365-2559.2005.02160.x (2005).
51 Scholzen, T. & Gerdes, J. The Ki-67 protein: from the known and the unknown. *J Cell Physiol* **182**, 311-322, doi:10.1002/(sici)1097-4652(200003)182:3<311::aid-jcp1>3.0.co;2-9 (2000).
52 Qin, R. *et al.* Combining clinicopathological predictors and molecular biomarkers in the oncogenic K-RAS/Ki67/HIF-1alpha pathway to predict survival in resectable pancreatic cancer. *British journal of cancer* **112**, 514-522, doi:10.1038/bjc.2014.659 (2015).